RWTH Aachen University

Master's Thesis

Semionic Resonating Valence Bond states on the kagome lattice

Author:
Mohsin Iqbal

Supervisor:
Prof. Dr. Norbert Schuch
Examiner:
Prof. Stefan Wessel, Ph.D.

A thesis submitted in fulfilment of the requirements for the degree of Masters in Simulation Sciences

in the

German Research School for Simulation Sciences

October 2013

Declaration of Authorship

I, Mohsin Iqbal, declare that this thesis titled, 'Semionic Resonating Valence Bond states on the kagome lattice' and the work presented in it are my own. I confirm that:

- This work was done wholly or mainly while in candidature for a research degree at this University.
- Where any art of this thesis has previously been submitted for a degree or any other qualification at this University or any other institution, this has been clearly stated.
- Where I have consulted the published work of others, this is always clearly attributed.
- Where I have quoted from the work of others, the source is always given. With the exception of such quotations, this thesis is entirely my own work.
- I have acknowledged all main sources of help.
- Where the thesis is based on work done by myself jointly with others, I have made clear exactly what was done by others and what I have contributed myself.

Signed: _____

Date: _____

RWTH AACHEN UNIVERSITY

Abstract

German Research School for Simulation Sciences

Masters in Simulation Sciences

Semionic Resonating Valence Bond states on the kagome lattice

by Mohsin Iqbal

The Heisenberg model is an effective Hamiltonian to describe the behavior of Quantum spin systems. Depending on the lattice geometries, the ground states of the system can carry different phases and can be differentiated qualitatively. Recent numerical studies using DMRG have shown a strong evidence that the ground states of the Heisenberg Hamiltonian on frustrated lattices exists as a $\mathbb{Z}_2$ spin liquid with topological order. Resonating valence bond (RVB) states have been proposed as an ansatz to study the spin liquid phase of Heisenberg Hamiltonian. RVB state exists in the same phase as Kiteav's toric (simplest model for a $\mathbb{Z}_2$ spin liquid). But, the numerical results for physical quantities such energy splitting in case of DMRG studies of Heisenberg Hamiltonian and Resonating valence bond states contradict each other. In this thesis, we propose a different ansatz state to explain the ground state properties of Heisenberg anti-ferromagnetic Hamiltonian on the kagome lattice, namely Semionic RVB state. Semionic RVB state maps to a $\mathbb{Z}_2$ spin liquid (Double Semion Model) with semionic excitations. We study the numerical properties and topological order in Semionic RVB state. The main tool for numerical simulations is Projected Entangled Pair States (PEPS) which provide an efficient description of Semionic RVB states and allow for high-precision numerical calculations of its physical properties.

Contents

Chapter 1

Motivation and Overview

Finding out the solution of Heisenberg model to describe the behavior of Quantum Spin systems is one of the most complicated problems in condensed matter physics. It is also one the problems that can be stated very simply: Given a system of N particles with spin operators $\boldsymbol{S}_i$ for each particle at site i, Hamiltonian of the system has the form:

$$\mathcal{H} = \sum_{\langle i,j \rangle} J_{ij} \boldsymbol{S}_i \cdot \boldsymbol{S}_j \tag{1.1}$$

where i, j represent the sites on the lattice and J_{ij} are exchange interaction strengths.

The problem is to find the ground state (GS) wavefunction and to qualitatively characterize its phase in the thermodynamic limit as $N \to \infty$, depending on the value of J_{ij} and lattice geometry. Among the many different possibilities, some possible configurations are following [1]:

- **Néel phase:** All spins in this phase are parallel (ferromagnet) or anti-parallel (anti-ferromagnet) to each other and the expectation value $\langle S_i^z \rangle \neq 0$ for each i. Any state in this phase has a broken symmetry with a long range order.
- **Valence bond solid (VBS):** Adjacent lattice sites in this phase pair up to form singlets (valence bonds). The whole state is defined as the tensor product of all singlets. VBS also represents a symmetry broken phase with short range entanglements.
- **Quantum Spin Liquid (QSL):** It is a disordered state of spin system. This phase has no broken symmetries but carry exotic topological order with fractionalized excitations.

Among the different phases mentioned above, QSL phase posses many counter-intuitive properties and opens up the possibility to implement fault tolerant quantum computing [2]. Numerical studies of $\mathcal{H}$ on frustrated lattices, such as the kagome lattice using Density Matrix Renormalization Group (DMRG) method give a strong evidence that the GS wavefunction of $\mathcal{H}$ is a disordered spin state and realizes a $\mathbb{Z}_2$ spin liquid.

Resonating Valence Bond states (RVB) have been considered as an ansatz to study the GS wave function of $\mathcal{H}$ in spin liquid phase [3]. Results of numerical interpolation have shown that RVB state is in the same phase as Quantum Dimer state. Quantum Dimer state is equivalent to the Toric Code state and both can be transformed into each other using local unitaries. And Toric code state is a $\mathbb{Z}_2$ spin liquid [4, 5]. So, RVB states are also in the spin liquid phase. But the scaling of physical quantities in case of RVB state is different from the one observed in the DMRG studies.

Semionic Resonating valence bond states make a different anstaz to study the ground state wavefunction of $\mathcal{H}$ on frustrated lattices. Semionic RVB state realizes a different kind of $\mathbb{Z}_2$ spin liquid with semionic excitations. The main goal of this thesis is to study the physical properties of these states and to characterize their topological order using the formalism of Projected Entangled Pair States (PEPS).

The structure of the thesis is as follows:

- In **Chapter 2** we introduce some background topics that are needed for successive studies. We explain the idea of Tensor Network States (TNS) and for $2d$ systems, Projected Entangled Pair States (PEPS).
- In **Chapter 3** we introduce some basic definitions and explain the idea of arrow representation for dimer coverings. Using arrow representation we describe a different way to interpret RVB states and extend that idea to introduce Semionic RVB states. We introduce PEPS representation of Normal/Semionic Resonating Valence Bond states and Dimer models.
- In **Chapter 4** we describe the basic setup for numerical studies of Semionic RVB states. Given the exponential nature of many body Hilbert space, even with PEPS formalism numerical studies of Semionic RVB states are hard. We introduced some optimization in section 4.2 that allows us to scale up the lattice size for numerical analysis. In section 4.3 we give a description of code design and implementation.
- In **Chapter 5** we show the results of numerical studies with detailed discussions on symmetries in PEPS description of Semionic RVB states, topological sectors of Semionic RVB wavefunctions and connections between Semionic RVB state and Double Semion model.

- In **Chapter 6** we summarize all the results from different numerical calculations.
- In **Appendix A** we give a brief overview of Toric code state and Double Semion model.

Chapter 2

Tensor Network States

Phenomena involving interacting quantum many body systems are probably the hardest problems in quantum mechanics. Understanding of such systems is essential to get a better control of these systems and to exploit these systems for quantum information purposes. There has been a significant effort to understand this problem by numerous physicists but still the mechanisms behind the phenomena like high T_c superconductivity, fractionalization of physical quantities and topologically ordered phases of matter are not clearly understood.

2.1 Tensor Network States

In non-relativistic settings, Schrodinger equation gives a mathematically complete description of the dynamics of many body systems. With the Schrodinger equation as the starting point several simplified (effective) models like Heisenberg model (in case of strongly correlated quantum spin systems) have been proposed. These models have been conjectured to reproduce the observed behavior of such systems. However with few exceptions these models have not been solved analytically and only numerical simulations can be used to determine the properties predicted by these models.

In the last decade ideas from quantum information like entanglement theory have been applied to develop better numerical methods for strongly correlated many body systems. These methods describe many body wavefunction as an interconnected network of local tensors [6].

Density Matrix Renormalization Group (DMRG) proposed in 1992 by Steve White was one of the first algorithms that exploited this tensor network(TN) structure. Although, current language of tensor networks (Matrix Product States) for DMRG was established

later. Recently DMRG have been extended to more general situations and new methods e.g. Time-Evolving Block Decimation (TEBD), Projected Entangled Pair States (PEPS), and Tensor Renormalization Group (TRG) have been developed based on the same ideas. TN methods represent the state of the art in many body simulations. And they have been employed to study wide variety of systems.

2.1.1 Entanglement Entropy

To exploit entanglement as a tool, the first step is to define a measure that quantifies entanglement between two systems. Entanglement entropy (EE) is one such measure. Given a bipartite system, its state can be written as,

$$|\psi\rangle = \sum_{ij} \psi_{ij} |i\rangle |j\rangle \tag{2.1}$$

Using singular value decomposition (SVD), $|\psi\rangle$ can be re-defined by orthonormal basis $|\alpha_L\rangle, |\alpha_R\rangle$ from left and right, such that:

$$|\psi\rangle = \sum_{\alpha} \lambda_\alpha |\alpha_L\rangle |\alpha_R\rangle \tag{2.2}$$

Using the sequence of singular values λ_α, the entanglement entropy is defined as,

$$S = -\sum_{\alpha} {\lambda_\alpha}^2 \; log({\lambda_\alpha}^2) \tag{2.3}$$

Expressing it through the reduced density matrix ρ_L,

$$\rho_L = \sum_{\alpha} {\lambda_\alpha}^2 |\alpha_L\rangle \langle\alpha_L| \tag{2.4}$$

$$S(\rho_L) = -Tr(\rho_L log(\rho_L)) \tag{2.5}$$

2.1.2 Entanglement in Quantum Many-Body Systems and Area Law

Wavefunction of an N-body quantum system is given by:

$$|\psi\rangle = \sum_{i_1 i_2 ... i_N = 1}^{d} c_{i_1 i_2 ... i_N} |i_1 i_2 ... i_N\rangle \tag{2.6}$$

where each site exists in d-dimensional Hilbert space, $|\psi\rangle$ is specified by d^N complex numbers, which is exponentially large in the number of particles. Not all states in the

Hilbert space of a many body system are equal. Realistic Hamiltonians tend to be local. Due to the locality of interactions, low energy eigenstates of gapped local Hamiltonians satisfy *Area law* [7]. Area law states that *the entanglement entropy of a subsystem A with the whole system S is proportional to the size of the boundary of the subsystem A,*

$$S(\rho_A) \propto |\partial A| \tag{2.7}$$

where $|\partial A|$ denotes the size of the boundary of A.

For instance, consider a "valence bond solid" (VBS) state with oriented bonds (singlets) between adjacent sites on $2d$ square lattice as shown in *Fig. 2.1.* EE for VBS is $log(2)$ times the number of bond cuts. So, EE for VBS is proportional to the size of region A.

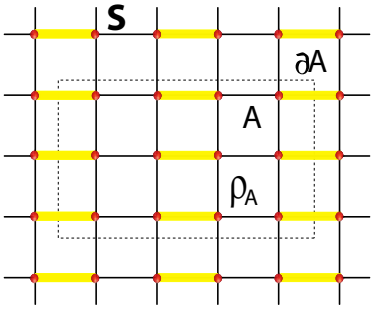

FIGURE 2.1: Valence Bond Solid: Yellow lines mark the singlet(valence bond) between adjacent spins. Region A in dashed line. EE of the region A is proportional to the number of number of bond cuts.

For a random quantum state we expect entanglement to be maximal, and EE between sub-regions will scale like volume and not as area. So entanglement properties can used to construct an ansatz class to parametrize the ground states of gapped local Hamiltonains.

2.1.3 Tensors and tensor network notation

A *tensor* is a multidimensional array of complex numbers. The *order* of the tensor is number of indices needed to specify the tensor. e.g. a scalar is an *order-0* tensor (C), a vector is an *order-1* tensor (v_i), and a matrix is an *order-2* tensor ($A_{i,j}$). The number of possible values an index can take is called the *size* or *dimensionality* of the index.

Tensor contraction is an operation that reduces the total order of a tensor by two. More precisely, it is the sum over all the possible values of the repeated indices of a set of tensors. Product of two matrices A and B,

$$C_{ik} = \sum_{j=1}^{D} A_{ij} B_{jk} \tag{2.8}$$

is a contraction over the index j. Similarly, contractions can be defined for multi-index tensors.

A *tensor network* is a tensor defined by a set of tensors linked together in the form of a graph. The number of indices that are not contracted defines the order of tensor network.

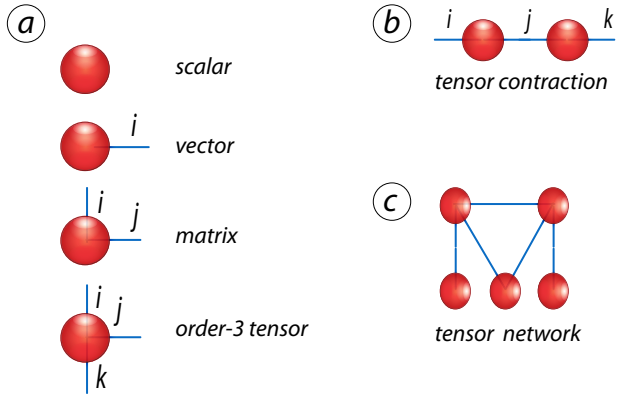

FIGURE 2.2: Tensor network diagrams:(a)Scalar, vector, matrix, and rank-3 tensor. (b)Tensor contraction over index j. (c)Tensor network.

2.2 Projected Entangled Pair States (PEPS)

Projected Entangled Pair States (PEPS) construct an ansatz class for all states in the Hilbert space of many body systems that obey area law. Here we consider the construction of PEPS in $2d$ on a square lattice. The following PEPS construction is based on steps described in [6].

2.2.1 Construction of PEPS

PEPS satisfy Area law and for any sub-region A, its entanglement with the rest of the system is concentrated around the boundary of the region. In order to satisfy this property for any bi-partition of the lattice, we decompose each site into four (number of neighboring sites) virtual subsystems, and place maximally entangled state $|\omega_D\rangle$ between adjacent sites,

$$|\omega_D\rangle = \frac{1}{\sqrt{D}} \sum_{i=1}^{D} |i\rangle\,|i\rangle \tag{2.9}$$

The resulting state has an Area law behavior, for any partition cut between two bonds. The next step is to apply a linear map from virtual system to real system. Map $\mathcal{P}^{[x,y]}$

$$\mathcal{P}^{[x,y]}: \quad \mathbb{C}^D \otimes \mathbb{C}^D \otimes \mathbb{C}^D \otimes \mathbb{C}^D \longrightarrow \mathbb{C}^d$$

is applied at each site $[x, y]$ to obtain the physical state on a $2d$ lattice of d-level systems.

$$|\psi_{peps}\rangle = \left(\mathcal{P}^{[1,1]} \otimes \mathcal{P}^{[1,2]} \ldots \otimes \mathcal{P}^{[N_x,N_y]}\right) |\omega_D\rangle^{\otimes N_x \cdot N_y} \tag{2.10}$$

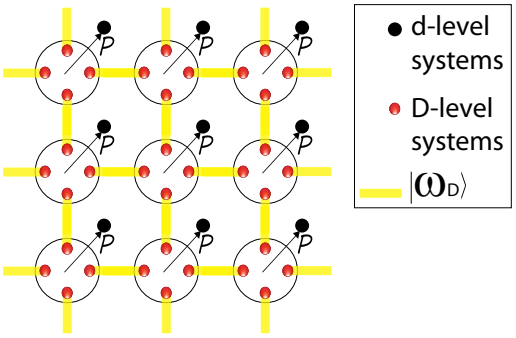

FIGURE 2.3: Construction of PEPS by applying maps $\mathcal{P}$ from virtual systems to physical systems

This creates a family of states which can be enlarged by increasing the bond dimension D. Each $\mathcal{P}^{[x,y]}$ can be specified by $D^4 \times d$ complex numbers. So PEPS is parametrized by $N \times D^4 \times d$ numbers, which has efficient scaling in the size of the system.

Each linear map $\mathcal{P}^{[x,y]}$ can be viewed in term of a five index tensor $A^{[x,y]}_{i,\alpha\beta\gamma\delta}$ as,

$$\mathcal{P}^{[x,y]} = \sum_{i,\alpha\beta\gamma\delta} A^{[x,y]}_{i,\alpha\beta\gamma\delta} \, |i\rangle \langle \alpha\beta\gamma\delta| \tag{2.11}$$

where $A^{[x,y]}_{i,\alpha\beta\gamma\delta}$ can be defined graphically as:

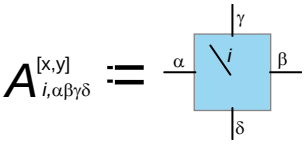

Using this graphical notation, coefficients $c_{i_{x1,y1},i_{x2,y1},\ldots}$ of PEPS as in [Eq. 2.6] can be interpreted as $2d$ tensor network of $A^{[x,y]}$,

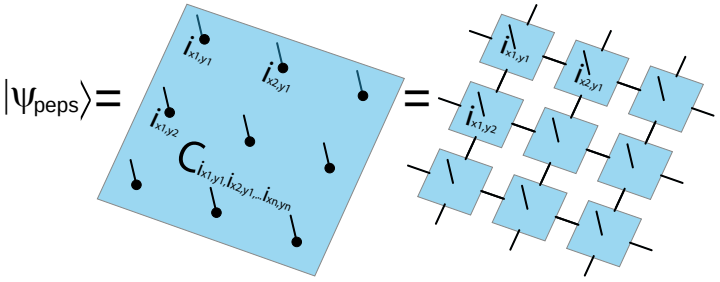

2.2.2 Calculation of Expectation values

To calculate the expectation value of local observables $\hat{O}$, e.g. $H = \sum h_i$, we define local expectation tensors, $\mathbb{E}$ and $\mathbb{E}_o$:

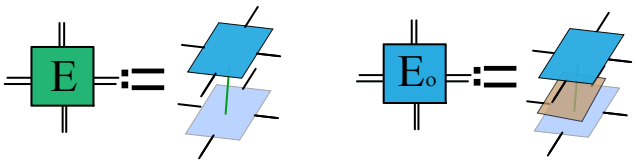

With $\mathbb{E}$ and $\mathbb{E}_o$, the computation of expectation value is reduced to the contraction of following tensor networks of the form:

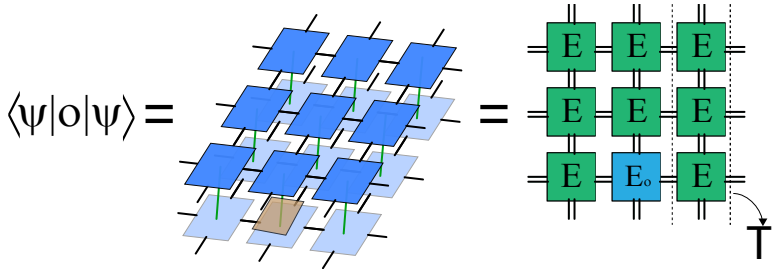

FIGURE 2.4: Graphical notation for the tensor network of expectation value. $\mathbb{T}$ is defined as the concatenation of $\mathbb{E}$'s in the vertical direction

To contract *2d* tensor network shown in *Fig. 2.4* for the calculation of expectation value we need to keep intermediate tensors with number of indices that is proportional to the $min(N_x, N_y)$. Storing such tensors require $D^{c.min(Nx,Ny)}$ complex numbers. The problem of finding the exact expectation values in case of PEPS belongs to the complexity class $\#P-$complete[24]. $\#P-$complete problems have no known polynomial time algorithm. Therefore, we need to rely on approximate contraction algorithms.

2.2.3 Properties of PEPS

In the following, we give some of the properties of PEPS:

- Ground states of gapped local Hamiltonian with realistic assumptions on spectral density can be approximated by a PEPS with

$$D_{max} = const \times \left[\left(\frac{N}{\epsilon}\right)\log\left(\frac{N}{\epsilon}\right)\right]^{c\times\log\left(\frac{N}{\epsilon}\right)} \tag{2.12}$$

  where $\epsilon := ||\psi_{exact}\rangle - |\psi_{peps}\rangle|$ [8].

- For any translationally non-invariant PEPS, one can do a translationally invariant PEPS construction by choosing a unit cell that is repeated over all the *2d* lattice [7].

- There exists PEPS that can handle power law decay of two point correlation function. Polynomial decay of the correlation function is a manifestation of infinite correlation length and scale invariance in critical systems. Hence PEPS makes a good candidate to represent the critical states of matter [9].

Chapter 3

Normal/Semionic Resonating Valence Bond States

Resonating valence bond (RVB) states were proposed by Anderson in 1987 as a wave-function to explain the mechanisms behind high-Tc superconductivity. They were also studied to give a description of disordering in Heisenberg anti-ferromagnets on frustrated lattices [3].

Roughly, RVB involves a state that is in a superposition of different ways to pair electrons into strongly-bonded spin singlets. One of the most interesting property of these states is that the excitations above them are fractional. These excitations carry one of the two key properties of electron. They could be electrically neutral $spin - 1/2$ fermonic excitations *spinons* or they could be $spin - 0$ charge excitations *visons*. Fractionalized excitations in RVB states are a manifestation of topological order.

3.1 The Basic Definitions and Concepts

3.1.1 Kagome lattice

Kagome is a $2d$ lattice with a network of corner-sharing triangles. *spin-1/2* particles are fixed at the vertices of the lattice with coupling constants ($J_{ij} > 0$) and interacts antiferromagnetically. An anti-parallel configuration could minimize the energy of each interaction between neighboring sites. However, this condition cannot be satisfied simultaneously for each pairwise interaction on kagome lattice and this leads to frustration. Frustration prevents spontaneous symmetry breaking in the underlying state on the lattice and makes an important candidate to realize a spin liquid phase [10]. An oriented kagome lattice is shown in *Fig. 3-1*.

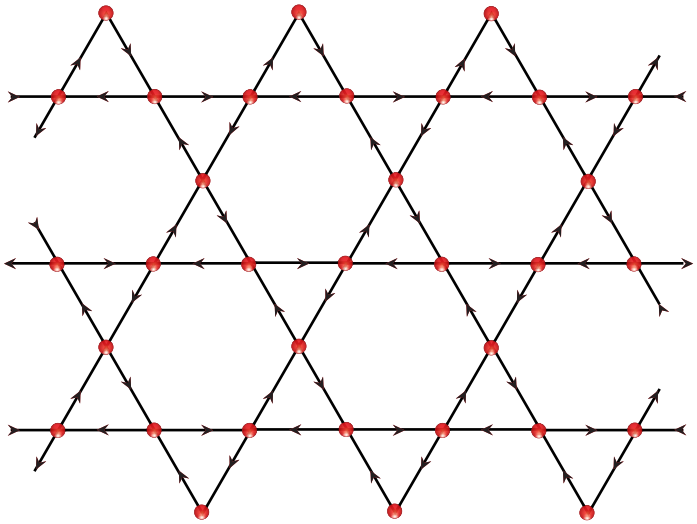

FIGURE 3.1: An oriented kagome lattice with *spin-1/2* particles at the vertices of the lattice.

3.1.2 RVB states

A *valence bond* is a **SU(2)** singlet state $|\uparrow\downarrow\rangle - |\downarrow\uparrow\rangle$, and it connects two $S = 1/2$ spins at sites a and b of the lattice. Given a lattice of atoms with qubits on each site with basis states $|0\rangle \equiv |\uparrow\rangle$ and $|1\rangle \equiv |\downarrow\rangle$, a nearest neighbor valence bond configuration or *singlet covering* $|\sigma(D)\rangle$ is a direct (tensor) product of valence bonds encompassing all the sites of the lattice.

$$|\sigma(D)\rangle = \prod_{i=1}^{N/2} \left(\left|\uparrow_{a_i}\downarrow_{b_i}\right\rangle - \left|\downarrow_{a_i}\uparrow_{b_i}\right\rangle \right) \tag{3.1}$$

The notation $|\sigma(D)\rangle$ followed here to represent a singlet covering has been adopted from [4] and the reason for use of D will be clarified in the next section. On an N-site lattice, a valence bond configuration $|\sigma(D)\rangle$ contains $N/2$ valence bonds. It is a spin configuration with total spin $\mathbf{S}^2_{tot} = S_{tot}(S_{tot}+1) = 0$.

Nearest Neighbor (NN) Resonating valence bond (RVB) state in the Hilbert space of many qubits is described as an equal weight superposition of all possible singlet coverings.

$$|\psi_{rvb}\rangle = \sum_{\sigma(D)\ \in\ coverings} |\sigma(D)\rangle \tag{3.2}$$

where the sum runs over all arrangements (coverings) of how to divide the lattice into pairs of adjacent lattice sites. *Fig. 3-2.* shows superposition of two possible singlet coverings on kagome lattice.

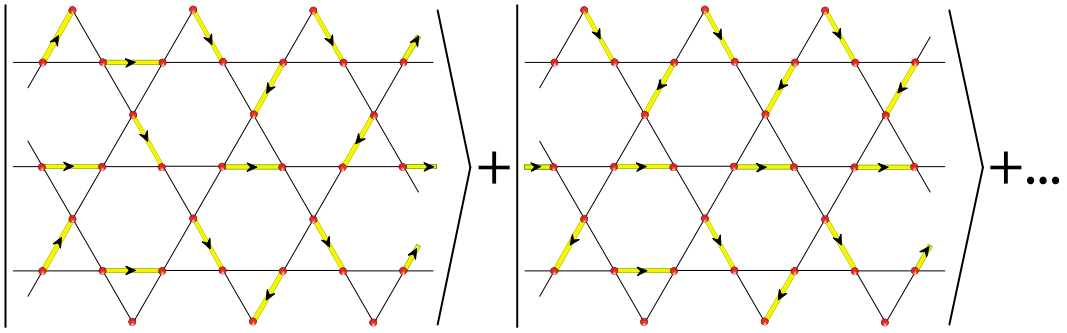

FIGURE 3.2: Pictorial representation of RVB state build from the superposition of singlet coverings on the kagome lattice. Yellow lines mark the singlets. Arrows on the yellow lines shows the orientation of singlets because singlets are anti-symmetric [22].

3.1.3 Quantum Dimer Models

Quantum dimer model was introduced by Rokhsar and Kivelson [23] to better understand and model the behavior of RVB states. Different singlet coverings in the RVB state are not orthogonal, e.g.,

$$\begin{array}{ccc} \bullet_1 & \cdots & \bullet_2 \\ \uparrow & & \downarrow \\ \bullet_3 & \cdots & \bullet_4 \end{array} \equiv |\sigma(D_1)\rangle = (|\uparrow_3\downarrow_1\rangle - |\downarrow_3\uparrow_1\rangle)\,(|\uparrow_2\downarrow_4\rangle - |\downarrow_2\uparrow_4\rangle) \tag{3.3}$$

$$\begin{array}{ccc} \bullet_1 & \rightarrow & \bullet_2 \\ \vdots & & \vdots \\ \bullet_3 & \leftarrow & \bullet_4 \end{array} \equiv |\sigma(D_2)\rangle = (|\uparrow_1\downarrow_2\rangle - |\downarrow_1\uparrow_2\rangle)\,(|\uparrow_4\downarrow_3\rangle - |\downarrow_4\uparrow_3\rangle) \tag{3.4}$$

It can be easily checked that $\langle\sigma\,(D_1)\,|\sigma\,(D_2)\rangle \neq 0$.

Quantum dimer model solves this problem by re-defining the system on the Hilbert space spanned by all dimer coverings with each two dimer coverings orthogonal by definition.

A *dimer* (a_i, b_i) is a state between adjacent vertices a_i and b_i on the lattice. A *dimer covering* is a direct tensor product of dimers encompassing all the sites on the lattice.

$$|D\rangle = \prod_{i=1}^{N/2} (a_i, b_i) \tag{3.5}$$

where dimers (a_i, b_i) between two vertices can be defined in different ways but it is more favorable to have a definition that ensures different dimer coverings D and D' to be locally orthogonal [4].

A *dimer state* is defined as an equal weight superposition of all dimer coverings on the lattice.

$$|\psi_{dimer}\rangle = \sum_{D \in coverings} |D\rangle \tag{3.6}$$

Quantum Dimer Models can describe following generic phases [11]:

- They realize dimer (or valence-bond) crystals with the long-range dimer-dimer correlations between the sites on the lattice.
- For certain geometries such as triangular and kagome lattices, spin-liquids.
- Critical spin liquids.

3.1.4 Arrow representation

For a dimer covering on kagome lattice as shown in *Fig. 3-2*, an alternate representation was introduced by Elser and Zeng [12]. They laid a pattern of arrows for each dimer on the kagome lattice that transformed a dimer covering on the kagome lattice into its dual honeycomb lattice. They placed an arrow at each vertex on the kagome lattice with a direction towards the center of one of the two neighboring triangles. The decision for choosing between two possible directions of arrow is governed by the *Arrow rule* which can stated as follow: *For each dimer* (i, j) *at an edge on kagome lattice the arrows at sites* i *and* j *must points towards the center of same triangle* [11].

For any dimer covering each triangle on kagome lattice can have at most one dimer. If a triangle has one dimer, it will have one outgoing and two incoming arrows. If a triangle has no dimer at any of its edges it will have three outgoing arrows in that case. The *Arrow rule* put a constraint on the parity of incoming (outgoing) arrows to be even (odd). *Fig. 3-3* gives a schematic description of the *Arrow rule*.

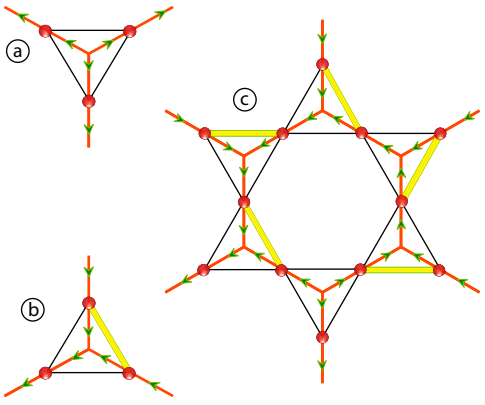

FIGURE 3.3: (a) A triangle without a dimer has three arrows pointing out. (b) On a triangle with a dimer, one arrow points out of the triangle and away from the dimer, the other two arrows point into the triangle. (c) Arrow patterns on kagome lattice generates a honeycomb lattice.

3.1.5 Dimer Coverings difference and Loop Patterns

Describing the dimer covering with the arrow representation gives a dual honeycomb lattice. Each link of the honeycomb lattice for a dimer covering has a fixed orientation decided by the direction of arrow (Arrow rule).

We fix a reference dimer covering or its dual arrow representation and denote it by R. For a given R, *strings* are defined as the edges on the honeycomb lattice where the difference of an arbitrary covering A and R has arrows pointing in the opposite direction.

As described in [sec. 3.1.4] the parity of outgoing arrows from each vertex on the honeycomb lattice is odd. For each vertex of the honeycomb lattice the difference of any two coverings either gives two edges with *strings* or none. This is true for all vertices. So, the difference of R and any arbitrary configuration A generates a *string pattern of closed loops*. Strings generated by all possible differences on a vertex is shown pictorially in *Fig. 3-4(a). Fig. 3-4(b)* gives an example of loop pattern generated by the difference of an arbitrary dimer covering A and R.

Loop patterns from dimer or singlet coverings can also be visualized as the assignment of *color* to a dual variable that exists inside each hexagon and strings can be interpreted as difference of color between two hexagons. There is a 2-to-1 mapping between colors assignment to hexagons and loop patterns since flipping the color in each hexagon also describes the same loop pattern. We will make use of this idea when we will describe the PEPS formalism in the next section.

3.1.6 Semionic Dimer and Semionic RVB states

Loop pattern description allows for an alternative interpretation of Dimer state and RVB state. We can interpret dimer (singlet) coverings in Dimer (RVB) state in the language of loop patterns. We define Semionic Dimer and Semionic RVB state in this language.

For a fix reference configuration R, we associate a loop pattern L to each dimer covering D and define *Semionic Dimer state* as a superposition of all possible dimer coverings with a phase factor that is determine by the parity of the number of closed strings in the loop configuration L.

$$|\psi_{sdimer}\rangle = \sum_{D \in covering} (-1)^{n(L)} |D\rangle \tag{3.7}$$

where $n(L)$ is the number of closed strings in the loop configuration L associated with dimer covering D.

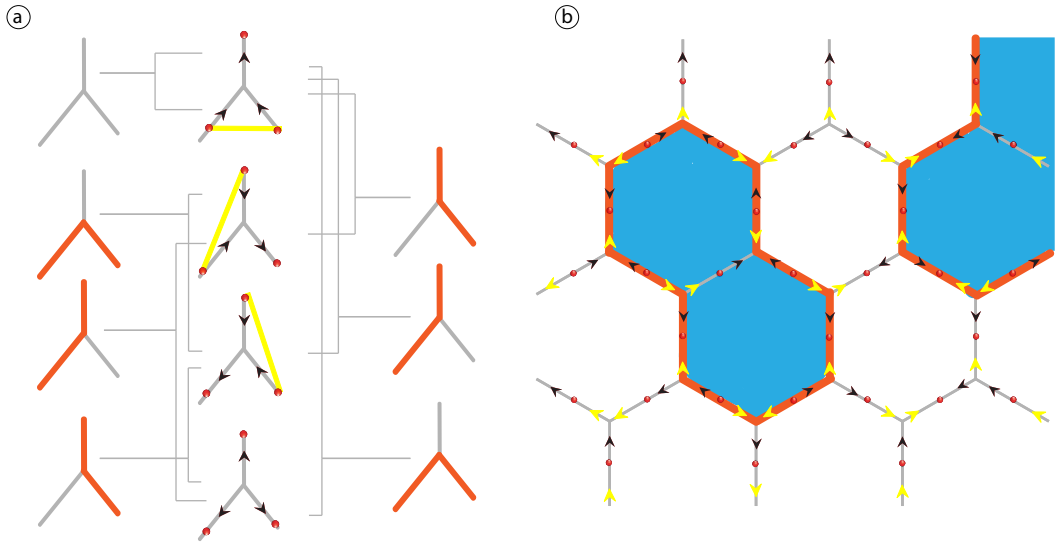

FIGURE 3.4: (a)Vertices in the middle column represent possible dimer or arrow configuration. Yellow lines mark the dimers. Vertices in the left and right columns represent the strings generated by the difference of two vertices in the middle column.(b)Yellow arrows represent a reference dimer covering R. Black arrows show an arbitrary converging A. String generated by the difference of R and A are shown by orange lines. Blue or white color of each hexagon shows the color assignment to the dual variable of hexagon.

In the same manner, for a fix reference configuration R, and with a map of each singlet covering $\sigma(D)$ to loop pattern L we define *Semionic RVB state* as a superposition of all possible singlet coverings with a phase factor that is determine by the parity of the number of closed strings in the singlet loop configuration L.

$$|\psi_{srvb}\rangle = \sum_{\sigma(D)\ \in\ covering} (-1)^{n(L)} |\sigma(D)\rangle \tag{3.8}$$

where $n(L)$ is the number of closed strings in the loop configuration L associated with singlet covering $\sigma(D)$.

3.2 PEPS formalism

PEPS representation for RVB state was first given in [9]. Subsequently, an alternative formalism was presented in [4] with detailed numerical studies of RVB state. Extending on [4], in this section we introduce a different PEPS representation for RVB state defined in terms of loop patterns. This PEPS representation can be easily altered to account for Semionic RVB state, Dimer state and Semionic Dimer state.

3.2.1 PEPS representation of RVB states

As introduced in previous section, a dimer configuration can also be represented by arrow notation. *Fig. 3-5* shows the arrow representation of the reference dimer covering R. All tripods within each triangle of kagome lattice creates a honeycomb lattice with physical sites at the center of each edge.

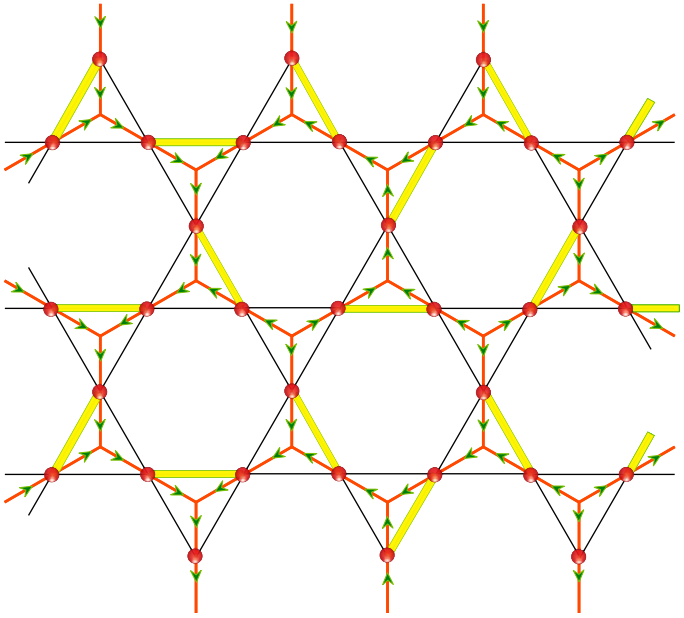

FIGURE 3.5: Arrow representation of dimer covering R. Yellow lines mark dimer between physical sites with corresponding green arrows.

The first step for the PEPS description of RVB state is the construction of virtual space. This is done by putting 2-qutrits *(3-level particles)* and 2-qubits *(2-level system)* on each physical site.

The next step is to insert entanglement by applying 3-qutrit state $|\epsilon\rangle$ in the clockwise direction at the center of each triangle on the kagome lattice or at the vertices of the honeycomb.

$|\epsilon\rangle$ is defined as,

$$|\epsilon\rangle := (|012\rangle - |102\rangle) + (|120\rangle - |021\rangle) + (|201\rangle - |210\rangle) + |222\rangle \tag{3.9}$$

$$= \sum_{i,j,k=0}^{2} \epsilon_{ijk} |ijk\rangle + |222\rangle \tag{3.10}$$

Next step is to put in $|\delta\rangle$ state between all the qubits inside a hexagon. $|\delta\rangle$ acts as a multi-index Kronecker delta with its legs connected to one of the qubits at the vertices of kagome lattice. As described in [sec. 3.1.5], given a reference dimer covering with a arrow representation R and an arbitrary dimer covering D with arrow representation A, we associate a loop pattern to D created by the difference of A and R. The loop

pattern of D can be interpreted as an assignment of color with two possible values to each hexagon. The color information indicates whether hexagon is inside a loop or not. Each leg of $|\delta\rangle$, $(i_1, i_2, i_3, i_4, i_5, i_6)$ has dimension 2 and it acts as a keeper for the color of each hexagon and ensures one color inside each hexagon for a given loop configuration.

$|\delta\rangle$ is defined as,

$$|\delta\rangle := \sum_{i_1 i_2 ... i_6 = 0}^{1} \delta_{i_1 i_2 ... i_6} \, |i_1 i_2 ... i_6\rangle \tag{3.11}$$

$|\delta\rangle$ is not necessary for the PEPS description of RVB state but there use becomes essential in case of Semionic RVB. *Fig. 3.6* shows a schematic version of $|\epsilon\rangle$ and $|\delta\rangle$.

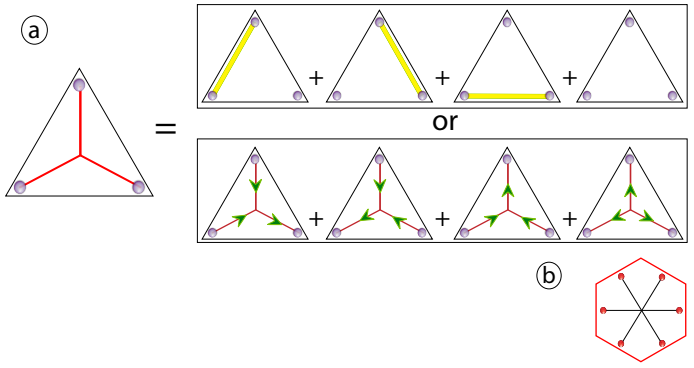

FIGURE 3.6: a)Mark two dimer and arrow representation of $|\epsilon\rangle$. b) shows $|\delta\rangle$, with six legs each one connected to one of the color qubits on the edge of each hexagon.

The net state of the virtual system is the direct tensor product of all $|\epsilon\rangle$'s and $|\delta\rangle$'s,

$$|\Omega_{rvb}\rangle = \prod_i |\epsilon\rangle_i \prod_j |\delta\rangle_j \tag{3.12}$$

where i runs over all vertices of the honeycomb lattice and j over all the hexagons.

The next step is to define a reference dimer configuration R on the kagome lattice which is equivalent to putting an arrow pattern on the edges of the honeycomb lattice. The resulting state of the virtual system is shown in *Fig. 3-7.*

Now we apply a linear map $\mathcal{P} : \left(\mathbb{C}^3\right)^2 \bigotimes \left(\mathbb{C}^2\right)^2 \to \left(\mathbb{C}^2\right)$ at the center of each link of the honeycomb lattice from virtual space to real space.

$$\mathcal{P} := |0\rangle \left[\langle 02| \left(\langle \blacksquare\square| + \langle \square\blacksquare|\right) + \langle 20| \left(\langle \blacksquare\blacksquare| + \langle \square\square|\right)\right] +$$

$$|1\rangle \left[\langle 12| \left(\langle \blacksquare\square| + \langle \square\blacksquare|\right) + \langle 21| \left(\langle \blacksquare\blacksquare| + \langle \square\square|\right)\right] \tag{3.13}$$

$$= \sum_{i=0}^{1} |i\rangle \left[{}_a\langle i|_b\langle 2| \left(\langle \blacksquare\square| + \langle \square\blacksquare|\right) +_a \langle 2|_b\langle i| \left(\langle \blacksquare\blacksquare| + \langle \square\square|\right)\right] \tag{3.14}$$

where filled and empty squares represents the state of the color qubits inside hexagons adjacent to $\mathcal{P}$.

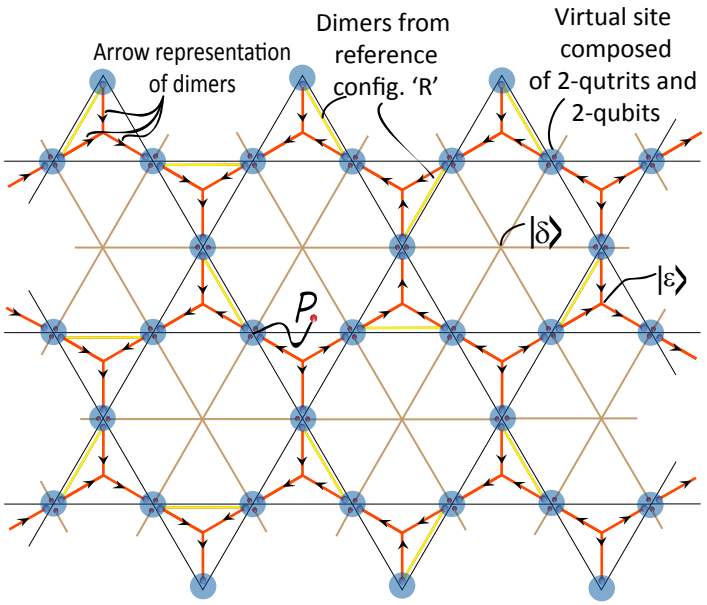

FIGURE 3.7: State of virtual system with $|\epsilon\rangle$ between qutrits and $|\delta\rangle$ between color qubits. Map $\mathcal{P}$ is applied at the center of each link on the honeycomb lattice. Map $\mathcal{P}$ is indicated at only one site to make the figure look less cluttered.

$\mathcal{P}$ is symmetric with respect to the exchange of color indices (qubits) but asymmetric with respect to the exchange of indices associated with qutrits. So, qutrits a and b are labeled such that a always comes in the direction of arrow of the reference configuration R. Therefore, whenever the arrows of an arbitrary configuration A and R points in the opposite direction the difference of A and R forms a loop and $\mathcal{P}$ projects only those configurations in virtual system which have opposite color on each side of the loop.

The PEPS description of RVB state is given by,

$$|\psi_{rvb}\rangle = (\mathcal{P})^{\otimes N} |\Omega_{rvb}\rangle \tag{3.15}$$

where N is the number of sites on the kagome lattice.

3.2.2 PEPS representation of Semionic RVB states

To get the right amplitude for each configuration we first introduced for each vertex on the honeycomb lattice 3-qubits, 1 for each neighboring hexagon. We next put in the state $|T\rangle$ between these qubits. The state $|T\rangle$ on each vertex of lattice looks at the color of neighboring hexagons and produces valid weighting factor by counting the number of left and right turns around any closed loop. $|T\rangle$ is defined as follows [13],

$$|T\rangle := \sum_{k=1}^{3} i \left(|1\rangle_k |00\rangle_{/k} - |0\rangle_k |11\rangle_{/k} \right) + |000\rangle + |111\rangle \tag{3.16}$$

$|T\rangle$ is shown schematically in *Fig. 3-8.* On going around any closed loop, product of all $|T\rangle$'s give a factor of *-1.*

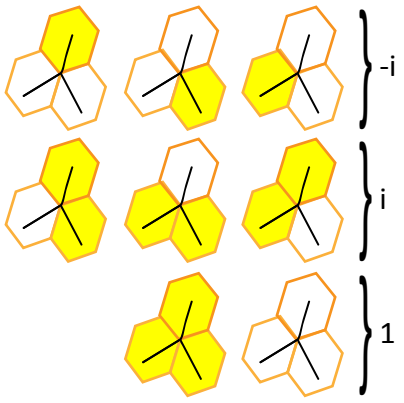

FIGURE 3.8: Action of T for different color configurations of neighboring hexagons.

In case of Semionic RVB state, we keep the same state $|\epsilon\rangle$ between the qutrits at each link of the honeycomb and the state $|\delta\rangle$ between color qubits at each edge of the honeycomb lattice.

The resulting virtual state $|\Omega_{srvb}\rangle$ is then given by the direct tensor product of all $|\epsilon\rangle$'s, $|\delta\rangle$'s, and $|T\rangle$'s.

$$|\Omega_{srvb}\rangle = \prod_{i,j,k} c_j \, |\epsilon\rangle_i |\delta\rangle_j |T\rangle_k \tag{3.17}$$

where index i and k for $|\epsilon\rangle$'s and $|T\rangle$'s runs over all the vertices of the honeycomb lattice and the index j of $|\delta\rangle$'s runs over all the hexagons. Coefficients c_j enforce an additional constraint and is defined as:

$$c_j := \delta_{j_1, j_2, \ldots j_{12}} \tag{3.18}$$

where $j_1, j_2, \ldots j_{12}$ represents the color qubits at each vertex and edge of the hexagon. c_j sync up (fix) the color of each of the 12 color qubits. $|\Omega_{srvb}\rangle$ is shown schematically in *Fig. 3-9.*

By applying the same map $\mathcal{P}$ as in case of RVB state to $|\Omega_{srvb}\rangle$ gives a PEPS description of Semionic RVB state.

$$|\psi_{srvb}\rangle = (\mathcal{P})^{\otimes N} \, |\Omega_{srvb}\rangle \tag{3.19}$$

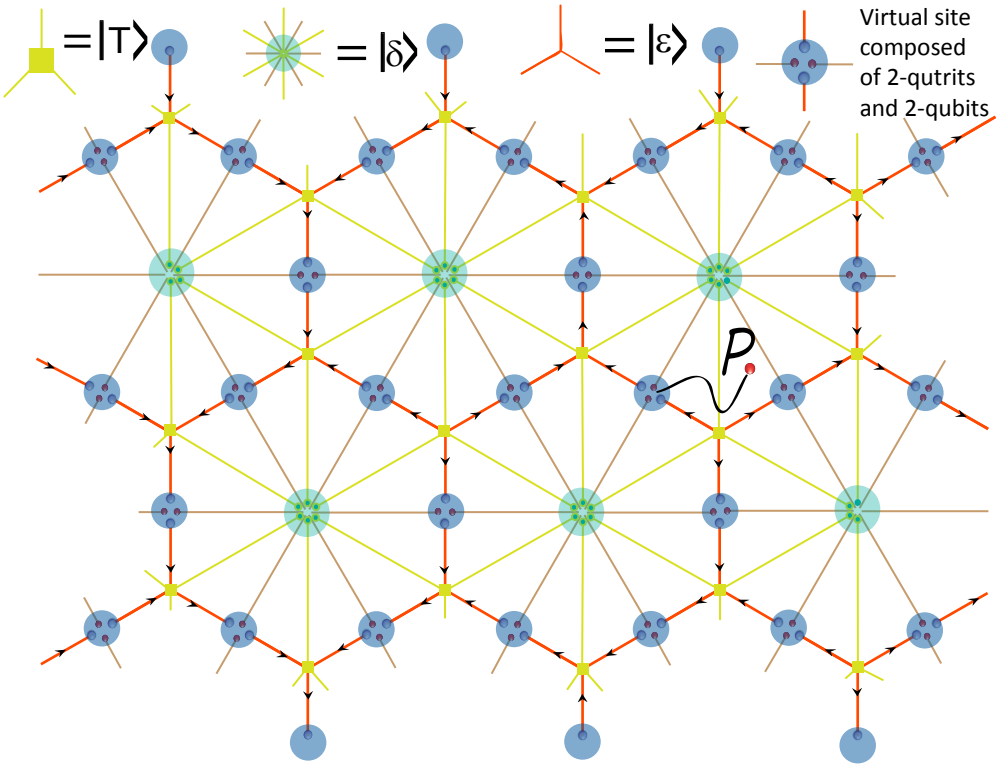

FIGURE 3.9: State of virtual system $|\Omega_{srvb}\rangle$ in case of Semionic RVB state, with $|\epsilon\rangle$ between qutrits and $|\delta\rangle$ between color qubits. State $|T\rangle$ is applied to color qubits at each vertex of the honeycomb. Map $\mathcal{P}$ is applied at the center of each link on the honeycomb lattice. Map $\mathcal{P}$ is indicated at only one site to make the figure look less cluttered.

3.2.3 PEPS representation of Dimer state and Semionic Dimer state

In [4], PEPS representation of orthogonal dimer state was presented by modifying dimensions of the physical sites from 2 to 9. Here we extend on the same work and re-define the map $\mathcal{P}_\perp : \left(\mathbb{C}^3\right)^2 \bigotimes \left(\mathbb{C}^2\right)^2 \rightarrow \left(\mathbb{C}^3\right)^2$, such that

$$\mathcal{P}_\perp = |02\rangle\left[\langle 02|\left(\langle \blacksquare\square| + \langle \square\blacksquare|\right)\right] + |20\rangle\left[\langle 20|\left(\langle \blacksquare\blacksquare| + \langle \square\square|\right)\right] +$$

$$|12\rangle\left[\langle 12|\left(\langle \blacksquare\square| + \langle \square\blacksquare|\right)\right] + |21\rangle\left[\langle 21|\left(\langle \blacksquare\blacksquare| + \langle \square\square|\right)\right] \tag{3.20}$$

$$= \sum_{i=0}^{1} |i2\rangle\left[{}_a\langle i|_b\langle 2|\left(\langle \blacksquare\square| + \langle \square\blacksquare|\right)\right] + |2i\rangle\left[{}_a\langle 2|_b\langle i|\left(\langle \blacksquare\blacksquare| + \langle \square\square|\right)\right] \tag{3.21}$$

where filled and empty squares represents the state of the color qubits inside hexagons adjacent to $\mathcal{P}_\perp$.

Although, each site has a 9 dimensional Hilbert space, $\mathcal{P}_\perp$ uses only 4 dimensions. By exploiting, this fact we can reduce it, $\mathcal{P}_\perp : \left(\mathbb{C}^3\right)^2 \bigotimes \left(\mathbb{C}^2\right)^2 \to (\mathbb{C})^4$

$$\mathcal{P}_\perp = \sum_{i=0}^{1} \left(|i\rangle + |i+2\rangle\right) \left[\langle i2| \left(\langle \blacksquare\square| + \langle \square\blacksquare|\right)\right] + \left(|i\rangle - |i+2\rangle\right) \left[\langle 2i| \left(\langle \blacksquare\blacksquare| + \langle \square\square|\right)\right] \tag{3.22}$$

This simplification is paramount in reducing the computation time when doing numerical interpolation between RVB and Dimer state.

By applying $\mathcal{P}_\perp$ on virtual states $|\Omega_{rvb}\rangle$ and $|\Omega_{srvb}\rangle$, we get PEPS description for orthogonal dimmer version of RVB state called Dimer state and for Semionic RVB state called Semionic Dimer state.

$$|\psi_{dimer}\rangle = \left(\mathcal{P}_\perp\right)^{\otimes N} |\Omega_{rvb}\rangle \tag{3.23}$$

$$|\psi_{sdimer}\rangle = \left(\mathcal{P}_\perp\right)^{\otimes N} |\Omega_{srvb}\rangle \tag{3.24}$$

Appendix A gives a brief overview of Toric code and Double Semion model. In [4], it has been shown rigorously that orthogonal Dimer state is equivalent to Toric code state and both can be transformed into each other using local unitaries. Using the same line of argument one show the equivalence of Semionic Dimer state and Double Semion model. Results of numerical interpolation between dimer state and RVB state shows that both of these states are in the same phase. Similar calculations for Semionic RVB state and Semionic dimer model has been performed in this thesis (see sec. 5.3).

Chapter 4

Implementation

4.1 Tensor Network Formalism of Semionic RVB state

An alternative description of Semionic RVB state can be given in terms of a tensor network composed of local tensors. Tensor network (TN) description is more convenient for the numerical analysis of problem. States $|\epsilon\rangle$, $|\delta\rangle$, and $|T\rangle$ that were used for the PEPS description of Semionic RVB can be formulated as multi-index tensors, such that,

$$|\epsilon\rangle := \sum_{\alpha,\beta,\gamma,=0}^{2} E^{\alpha\beta\gamma} |\alpha\beta\gamma\rangle \tag{4.1}$$

where $E^{\alpha\beta\gamma}$ is an order-3 tensor and each index has a dimension of 2. $E^{\alpha\beta\gamma}$ is anti-symmetric with respect to the exchange of indices.

State $|T\rangle$ is given by [13],

$$|T\rangle := \sum_{j,k,l=0}^{1} T_{jkl} |jkl\rangle \tag{4.2}$$

where,

$$T_{jkl} = \begin{cases} 1 & if \quad j+k+l = 0,3 \\ i & if \quad j+k+l = 1 \\ -i & if \quad j+k+l = 2 \end{cases} \tag{4.3}$$

with $j, k, l = 0, 1$.

$|\delta\rangle$ can be viewed as 12-index tensor $\delta_{i_1 i_2 \ldots i_6 j_1 j_2 \ldots j_6}$ each leg has dimension 2.

Projector $\mathcal{P}$ is defined by,

$$\mathcal{P} := \sum_{i,j,k=\{0,1\},\eta,\vartheta=\{0,1,2\}} P^{i}_{\eta\vartheta,jk} \left|i\right\rangle \left\langle\eta\vartheta\right| \left\langle jk\right|, \tag{4.4}$$

where,

$$P^{i}_{\eta\vartheta,jk} = \begin{cases} 1 & if \quad (i=\eta=0,1 \quad \wedge \quad \vartheta=2) \quad \wedge \quad j=k \\ 1 & if \quad (i=\vartheta=0,1 \quad \wedge \quad \eta=2) \quad \wedge \quad j\neq k \\ 0 & otherwise \end{cases} \tag{4.5}$$

η, ϑ, j, and k represents inner legs and have dimensions of $3, 3, 2$ and 2. i represents an outer leg and has a dimension of 2.

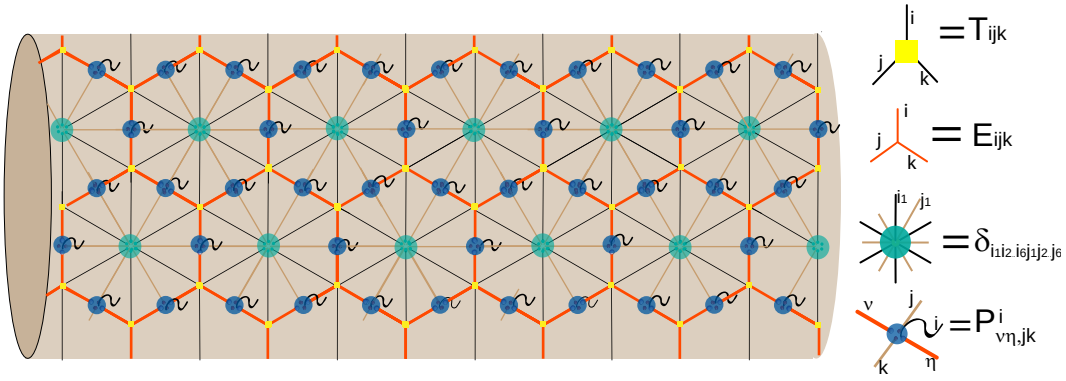

FIGURE 4.1: Tensor network of Semionic RVB state on honeycomb with cylindrical topology

Semionic RVB wavefunction can be defined as a summation over all the virtual indices on the shared links in the tensor network shown in *Fig. 4-1.*

$$\left|\psi_{srvb}\right\rangle = \sum_{i_1,i_2,\ldots=0}^{1} tTr\left(\underset{i}{\otimes} T_i \underset{j}{\otimes} \delta_j \underset{k}{\otimes} E_k \underset{l}{\otimes} P_l\right) \left|i_1, i_2, \ldots\right\rangle \tag{4.6}$$

where tTr (tensor trace) is defined as in [13] by doing the sum over all the open indices in the virtual layer of the tensor network.

Semionic RVB wavefunction has by definition a non-local description. Closed strings in a given loop pattern are large objects and can extend up to the size of the system. Finding the parity of the number of closed strings seems like a global operation. But, tensor network formulation still enables us to give a description of Semionic RVB state in terms of local tensors [13].

4.2 Block decomposition and abstractions

Tensor network of Semionic RVB state roughly forms a honeycomb lattice. Also implemented in [4], from implementation perspective it is very useful to block 3-spins moments together with 2-E, 2-T and 3-δ tensors as shown in *Fig. 4.2(a,b)*. By doing this, we convert honeycomb TN into square TN.

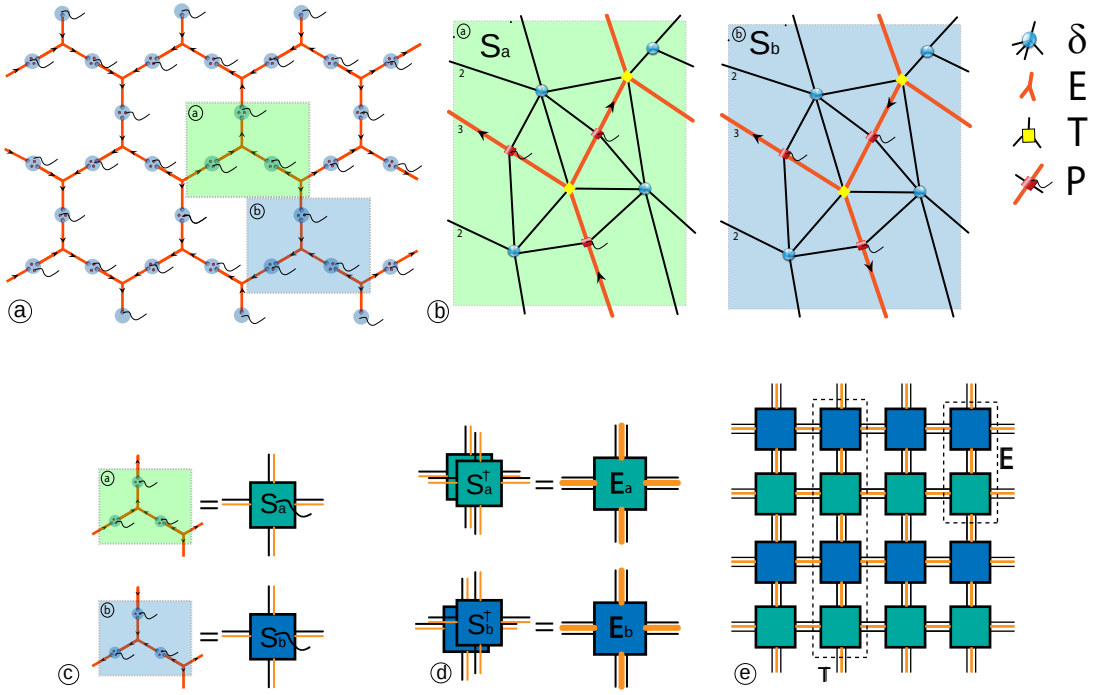

FIGURE 4.2: (a) Tensor network of Semionic RVB state. Squares labeled a. and b. marks two blocks of 3-physical sites with different arrows of reference configuration R.(b) Blocks a. and b. with internal structure. (c) Blocks a. and b. defined as S_a and S_b. S_a and S_b converts honeycomb into square TN. (d) Sandwiching S_a and S_b with their conjugates ${S_a}^\dagger$ and ${S_b}^\dagger$ gives $\mathbb{E}_a$ and $\mathbb{E}_b$. (e) Tensor network of $\langle\psi_{srvb}|\psi_{srvb}\rangle$

For a random reference singlet (dimer in case Semionic Dimer model) covering or loop configuration R, the square TN of Semionic RVB state is not translationally invariant. In order to get a TN description that is translationally invariant we need to choose a reference configuration R that must be translationally invariant with a block (unit cell) of certain size. For a reference configuration to be translationally invariant it can be shown by exhaustive search that the minimum block S must contain atleast six physical sites on the honeycomb lattice. For getting better performance during numerical calculations we divide the S into two sub-blocks S_a and S_b each containing 3-physical sites.

TN of Semionic RVB state is composed by repeating two blocks (tensors) S_a and S_b either horizontally or vertically. For remaining discussion, we will consider the vertical case. TN for the calculation of wavefunction normalization is shown in *Fig. 4.2(e)*.

Vertical stack of S_a and S_b tensors is shown in (*Fig. 4.3*). By using δ tensors labeled as $(1), (2), (3)$ and (4) S_a and S_b blocks ensure one color inside each hexagon. One of the constraint implemented by doing contraction on the leg labeled "d" is redundant and can be removed. This redundancy can be shown by the following relation:

$$\underbrace{\left(\delta^{(4)}\delta^{(1)}\right)}_{a}\underbrace{\left(\delta^{(1)}\delta^{(2)}\right)}_{b}\underbrace{\left(\delta^{(2)}\delta^{(3)}\right)}_{c}\underbrace{\left(\delta^{(3)}\delta^{(4)}\right)}_{d} = \underbrace{\left(\delta^{(4)}\delta^{(1)}\right)}_{a}\underbrace{\left(\delta^{(1)}\delta^{(2)}\right)}_{b}\underbrace{\left(\delta^{(2)}\delta^{(3)}\right)}_{c} \tag{4.7}$$

Removal of legs marked by "×" in (*Fig. 4.3*) reduces storage requirements of S_a and S_b by the factor of 4.

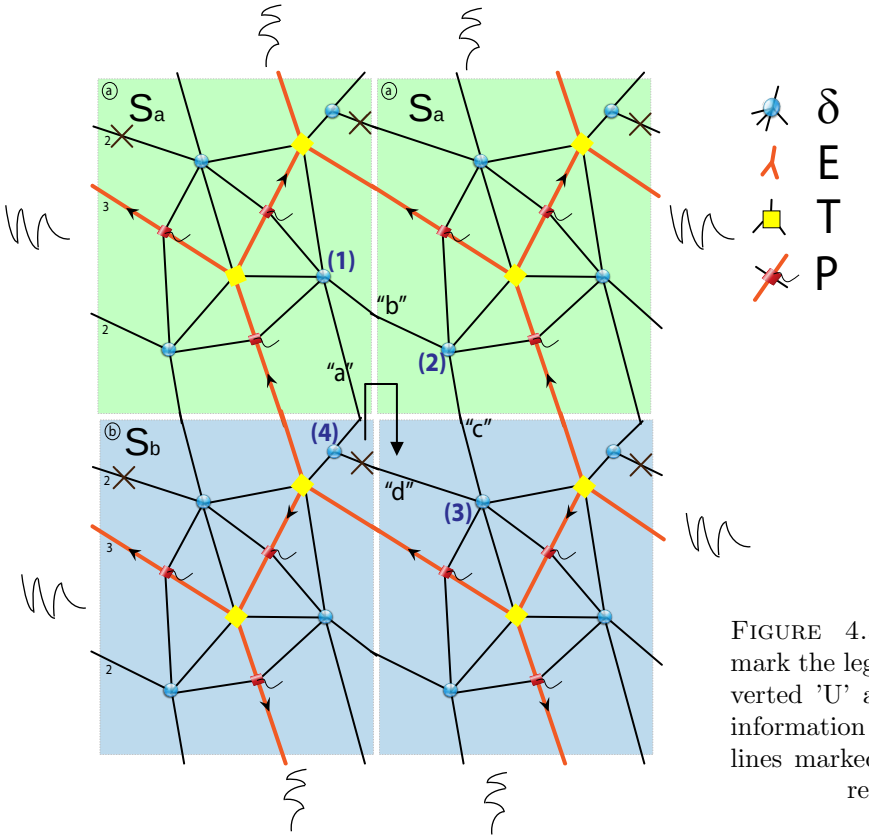

FIGURE 4.3: Black lines mark the legs of δ tensor. Inverted 'U' arrow shows how information is propagated, so lines marked with × can be removed.

4.3 Optimization

For the tensor network description of the block given in previous section, it requires $(3 \times 2)^2 \times \left(3 \times 2^2\right)^2 \times 2^3 \approx 10^5$ complex numbers to store S_a or S_b. This huge memory requirement just to store these local tensors creates a bottleneck even if we want to scale up to four blocks. In this section we will describe following two ways to resolve the scalability problem to some extent.

- An efficient tensor network description of S_a or S_b blocks.
- Applying isommetries to $\mathbb{E}$.

4.3.1 Efficient description of S_a or S_b Tensors

For a reference configuration R, δ tensor within each hexagon of honeycomb fixes its color and

- it ensures that given the color of the neighboring hexagons, $\mathcal{P}$ at shared edges projects into right subspace.
- it is used as a sensor by T tensors to get the right amplitude for the configuration.

If the color of one of the hexagon is fixed by δ, $\mathcal{P}$ and reference configuration R also freeze up the color of all neighboring hexagons, and this effect is propagated via E tensors (which have the information of loop strings) from first neighboring hexagons to the second neighboring hexagons and so on. This propagation of information from one end of the lattice to the other is ensured if all the δ tensors within each hexagon of honeycomb lattice are sufficiently connected.

Given the tensor network shown in *Fig. 4.3*, in the horizontal direction only one line of δ tensor legs in S_b blocks is sufficient. From the remaining of S_a and S_b tensors outgoing δ tensor legs in the horizontal direction can be removed without any impact.

The same optimization can also be applied in vertical direction but here the removal of one of the δ legs from the top right corner and bottom right corner would affect the function of T tensor.

Given a reference configuration R, for any arbitrary configuration A, T tensors at each vertex of the honeycomb lattice look at the color of neighboring hexagons to generate the right phase factor for A. The removal of δ tensor legs makes the color information inaccessible. This problem can be circumvented by putting in a COPY tensor (three leg delta each of size three) on the outgoing leg of top E tensor and CNOT tensor as shown in *Fig. 4.4*. Copy tensor gives the direction of arrow of A on the link of honeycomb. CNOT is defined depending on the direction of arrow of R on the same link. CNOT uses input from COPY tensor as a control line and do a controlled flip. T tensors uses the information from CNOT and generate the right phase factor.

COPY tensor is defined as:

$$COPY = \delta_{ijk} \tag{4.8}$$

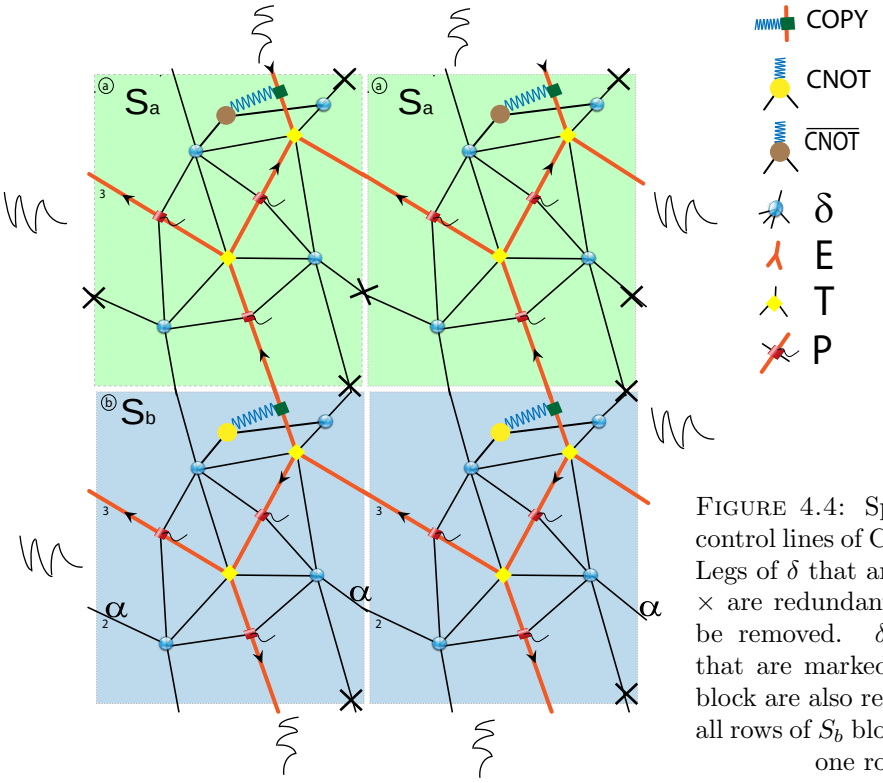

FIGURE 4.4: Springs act as control lines of CNOT tensor. Legs of δ that are marked by $\times$ are redundant and should be removed. δ tensor legs that are marked by α in S_b block are also removed in the all rows of S_b blocks except in one row.

CNOT is a three leg tensor with two legs of dimension two and one leg of dimension three. CNOT is symmetric to the exchange of 2 dimensional legs. It is defined depending on the direction of reference configuration R arrow. On the line where copy tensor is applied, if the arrow is going away from copy tensor then,

$$CNOT^{i}_{\alpha,\beta} := \begin{cases} 1 & if \quad (i = 0, 1) \wedge (\alpha = \beta) \\ 1 & if \quad (i = 2) \wedge (\alpha \neq \beta) \\ 0 & otherwise \end{cases} \tag{4.9}$$

otherwise,

$$CNOT^{i}_{\alpha,\beta} := \begin{cases} 1 & if \quad (i = 0, 1) \wedge (\alpha \neq \beta) \\ 1 & if \quad (i = 2) \wedge (\alpha = \beta) \\ 0 & otherwise \end{cases} \tag{4.10}$$

Now removing one of the legs of δ tensor from top/bottom of S_a and S_b blocks gives tensor network description of S_a and S_b shown in *Fig. 4.4*.

Applying these two optimization gives an overall reduction in memory requirements by the factor of 16 for each S_a and S_b block.

4.3.2 Applying Isometries to $\mathbb{E}$

Given the tensor network composed of local tensors $\mathbb{E}_{\alpha\beta\gamma\delta}$, to do the exact calculation for expectation values of local observables we need to store intermediate tensors with number of indices that are proportional to the number of $\mathbb{E}$ blocks along the circumference of cylinder. However, $\mathbb{E}_{\alpha\beta\gamma\delta}$ are not full rank tensors for indices α, β in case of Semionic RVB state and there are alternative ways for describing same TN.

$$\mathbb{E}_{\alpha\beta\gamma\delta} \longleftrightarrow X_{\alpha\alpha'} Y_{\beta\beta'} \mathbb{E}_{\alpha'\beta'\gamma'\delta'} {X^{-1}}_{\gamma\gamma'} {Y^{-1}}_{\delta\delta'} \tag{4.11}$$

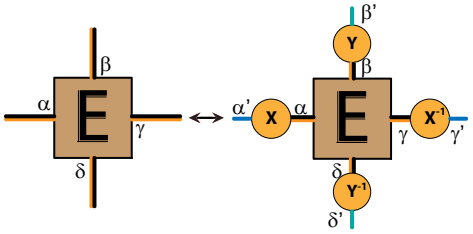

Isometries X and Y are calculated by using Singular Value Decomposition (SVD). By applying SVD on $\mathbb{E}_{\alpha\beta\gamma\delta}$ with indices α and (β, γ, δ),

$$\mathbb{E}_{\alpha;\beta\gamma\delta} = \sum_{\lambda,\mu} (U_x)_{\alpha,\lambda} S_{\lambda,\mu} \left(V_x^\dagger\right)_{\mu,(\beta\gamma\delta)} \tag{4.12}$$

where λ runs from 1 to the rank of index α and k from 1 to $(size(\beta) \cdot size(\gamma) \cdot size(\delta))$, and U_x is an isometry,

$$\sum_{\alpha} (U_x)_{\alpha,\lambda} \left(U_x^\dagger\right)_{\alpha,\mu} = \delta_{\lambda\mu} \tag{4.13}$$

Similarly, by applying SVD on indices β and (α, γ, δ), we get

$$\mathbb{E}_{\beta;\alpha\gamma\delta} = \sum_{\lambda,\mu} (U_y)_{\beta,\lambda} S_{\lambda,\mu} \left(V_y^\dagger\right)_{\mu,(\alpha\gamma\delta)} \tag{4.14}$$

with isometry,

$$\sum_{\beta} (U_y)_{\beta,\lambda} \left(U_y^\dagger\right)_{\beta,\mu} = \delta_{\lambda\mu} \tag{4.15}$$

Using, TN notation both SVD's can be shown figuratively as:

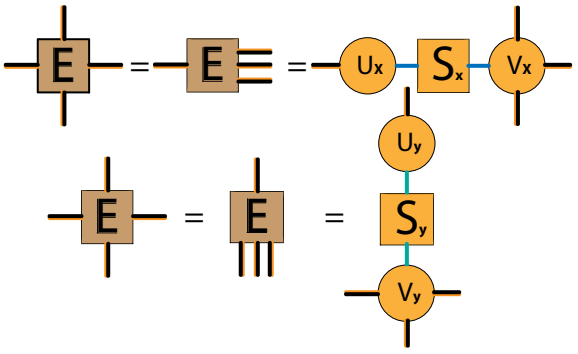

Applying theses isometries leads to reduced size for different contractions. Special care is needed to apply these isometries across sites on the tensor network where local operators act. *Fig. 4.5(a,b,c)* gives one example where local operator are sandwiched in diagonally adjacent blocks. For the case of Semionic RVB state application of isometries significantly reduces the size of indices both in the horizontal and vertical direction and allows for doing calculations upto 4 $\mathbb{E}$ blocks.

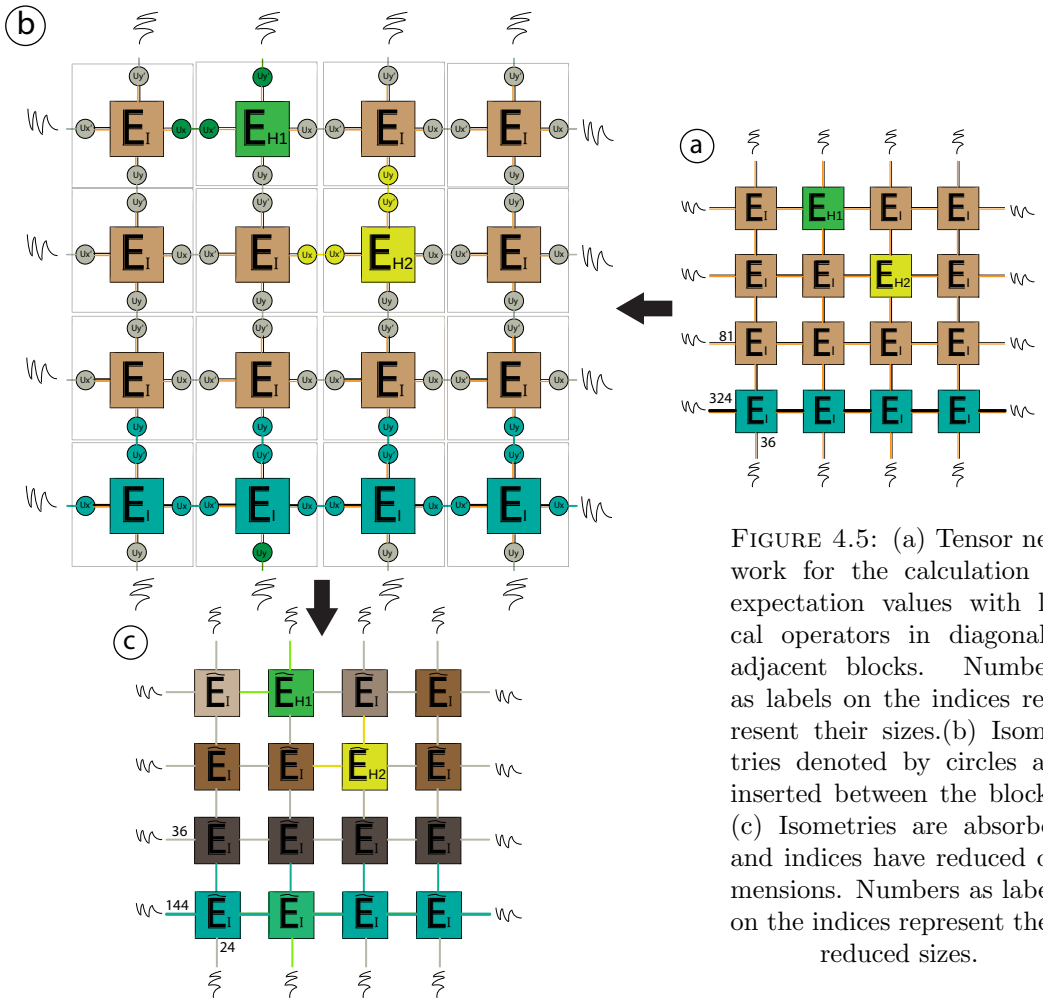

FIGURE 4.5: (a) Tensor network for the calculation of expectation values with local operators in diagonally adjacent blocks. Numbers as labels on the indices represent their sizes.(b) Isometries denoted by circles are inserted between the blocks. (c) Isometries are absorbed and indices have reduced dimensions. Numbers as labels on the indices represent their reduced sizes.

4.4 Description of Basic Procedures

Implementation for doing numerics with Semionic RVB states has been done in Matlab. Matrix-matrix and matrix-vector multiplication are the two main operations during tensor network contractions and consumes a major chunk of all processor cycles. So no significant reduction in the whole computation time can be achieved by doing implementation in high performance programming languages like C or Fortran. Parallel programming using MPI can be used to implement matrix-matrix and matrix-vector multiplication operations on a distributed computing environment (cluster). But given the large sizes of tensors, communication overhead would diminish any performance gains.

The whole execution cycle follows through by multiple execution of some basic procedures as it leads to the end results. In this section we will show the code snippets of basic these procedure and discuss their implementation.

Definition of primary tensors that are then composed to from tensor network of Semionic RVB states is described in the following code snippet:

```
function eps = epsilon
        % epsilon tensor
        eps = zeros(3,3,3);  % antisym + |222>
        eps(1,2,3)= 1; eps(2,3,1)= 1; eps(3,1,2)= 1;
        eps(3,2,1)=-1; eps(2,1,3)=-1; eps(1,3,2)=-1;
        eps(3,3,3)= 1;
end
function T=tripod
        % T tensor
        T = ones(2,2,2);
        T(1,1,2)=1i; T(1,2,1)=1i; T(2,1,1)=1i;
        T(1,2,2)=-1i; T(2,1,2)=-1i; T(2,2,1)=-1i;
end
function P=projector
        % indices 1 and 2 are the singlet bonds, indices 3 and 4 the plaquette
        % colors.  3!=4, then the physical index (=5) equals the 1-singlet,
        % otherwise (if 3==4) the 2-singlet
        P=zeros(3,3,2,2,2);
        % 3!=4: pick the first index
        P(1,3,1,2,1) = 1; P(2,3,1,2,2) = 1; P(1,3,2,1,1) = 1; P(2,3,2,1,2) = 1;
        % 3==4: pick the second index
        P(3,1,1,1,1) = 1; P(3,2,1,1,2) = 1; P(3,1,2,2,1) = 1; P(3,2,2,2,2) = 1;
end
function del = delta(N,dim)
        % N of legs in the delta tensor
        % dimension of each leg
                del=zeros(zeros(1,N)+dim);
        for i=1:dim
                currdim=num2cell(zeros(1,N)+i);
                del(currdim{:})=1;
        end
```

```
end
function CN = cnot
        % middle index acts as control qtrit,
        % 1st index act as input qubit, 3rd index as output qubit
        cpop=ones(2,3,2);
        cpop(1,1,2)=0; cpop(2,1,1)=0; cpop(1,2,2)=0; cpop(2,2,1)=0;
        cpop(1,3,1)=0; cpop(2,3,2)=0;
        CN = cpop;
end
```

LISTING 4.1: Definitions of basic tensors that are use to define Semionic RVB state

Primary tensors are then blocked to construct S_a and S_b tensors with different reference arrows. S_a and S_b are composed with/without δ tensor legs in the horizontal direction. Listing 4.2 shows one such construction.

```
SRVBTensor1Bot=scon({eps,eps,P,P,P,T,T,...
  delta(5,2),delta(5,2),delta(6,2),delta(2,2),delta(3,3),cnot}, ...
  {[4 9 11],[14 -5 17], ... % epsilons
   [[-7 4] 3 6 -9], [[14 9] 13 7 -10],[[11 -1] 1 12 -11], ...  % the P's
   [2 5 10],[16 8 15], ... % the T's
   [-8 -2 1 2 3],[-6 6 5 7 8],[-4 12 10 13 15 19],[16 20],[17 -3 18], ... %deltas
   [19 18 20]}) ... %  cnot
```

LISTING 4.2: Blocking of basic tensors to form a block S_b with outgoing δ tensor legs in horizontal direction

scon function takes as an input a list of tensors, list of tensor indices to be contracted and the order list for doing indices contractions as an optional parameter. Legs to be contracted are labeled by positive integers and legs of the resulting tensor are labeled by negative integers.

S_a and S_b tensors are then contracted with identity or local operators sandwiched in the ket and bra layer to construct $\mathbb{E}_a$ and $\mathbb{E}_b$ using *scon* function.

```
function SRVBE=rvb_lambda_split(SRVBTensor,ops)
  indx=size(SRVBTensor).*size(SRVBTensor);
  SRVBE=permute(reshape(
        scon({SRVBTensor,conj(SRVBTensor),... % bra and ket SRVB tensor
              ops{1},ops{2},ops{3}},...       % ops
             {[-1 -3 -5 -7 1 2 3],[-2 -4 -6 -8 4 5 6],[1 4],[2 5],[3 6]}),...
       [indx(1) indx(2) indx(1) indx(2)]),[1 3 2 4]);
end
```

LISTING 4.3: Contraction of S_a and S_b in the ket and bra layer to form $\mathbb{E}_a$ or $\mathbb{E}_b$

$\mathbb{E}_a$ are $\mathbb{E}_b$ contracted to form $\mathbb{E}$ blocks as shown in *Fig. 4.2(e)*. $\mathbb{E}$ forms a TN as shown in *Fig. 4.5(a)*.

Isometries are calculated for the $\mathbb{E}$ tensors to do compression on the tensor network.

```
function [Isometry, IsomRank] = calculate_isometry(tensor, whichIndices)
    % whichIndices:  specify the index for which isometry has to be calculated
    % tensor: input tensor
    tenSize=size(tensor);
    permutList=[whichIndices setdiff(1:length(tenSize),whichIndices)];
    tensor = reshape(permute(tensor,permutList),[prod(tenSize(whichIndices))
    numel(tensor)/prod(tenSize(whichIndices))]);

    [Isometry,D]=eig(tensor*tensor');
    [~,I]=sort(abs(diag(D)),'descend');
    IsomRank = rank(D);
    Isometry=Isometry(:,I(1:IsomRank));
end
```

LISTING 4.4: Calculates an insometry of tensor for indices specfied as input

Horizontal and vertical isometries are then applied to the $\mathbb{E}$ tensors that leads to the compressed local tensors. Given the compressed $\mathbb{E}$, the eigenvalues and eigenvectors of the transfer operator $\mathbb{T}$ (shown in *Fig. 4.2(e)*) are calculated using Lanczos algorithm. Lanczos algorithm is an iterative method and an adaptation of power algorithm to calculate the eigenvalues and eigenvectors of a square matrix.

During each Lanczos iteration, $\mathbb{T}$ is applied to a vector followed by other steps. With large N_v (number of $\mathbb{E}$ blocks along the circumference of cylinder), $\mathbb{T}$ and vector multiplication is a very expensive operation both in terms memory and computation time. To get better trade offs between cost (memory requirements) and performance (computation time), top and bottom legs of the transfer operator are traced over in a *for loop*. And during $\mathbb{T}$ and vector multiplication two legs of every local tensor $\mathbb{E}$ in $\mathbb{T}$ are contracted simultaneously. *Fig. 4.6* shows the schematic of steps followed in vector multiplication with $\mathbb{T}$. Contraction of two indices of $\mathbb{E}$ simultaneously is efficient both in terms of memory and computation time as compared to two separate contractions that require the storage of intermediate tensor with larger size.

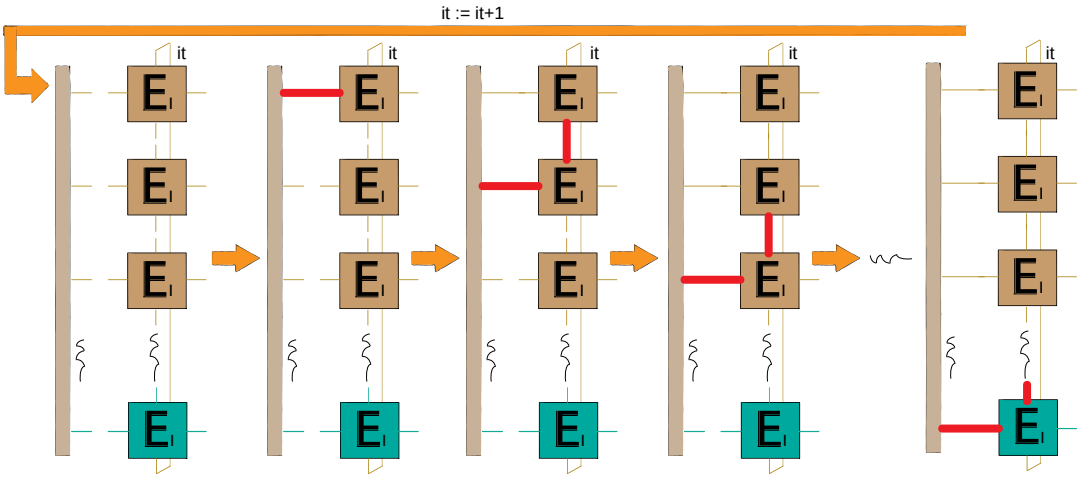

FIGURE 4.6: Steps followed in vector multiplication with $\mathbb{T}$ during each iteration of Lanczos algorithm. In the TN before the first small arrow, the thin vertical bar represents the vector and column of $\mathbb{E}$ tensors represents transfer operator $\mathbb{T}$. At each step indicated by small arrow, two legs of $\mathbb{E}$ marked by thick red lines are contracted simultaneously with the corresponding indices of vector. Index of $\mathbb{E}$ with the label "it" is traced over in a *for loop* and it ends in cycles that are equal to the size of that index. The whole cycle of steps followed by the small arrows is repeated until the *for loop* terminates.

Left and right eigenvectors of $\mathbb{T}$ are then used for calculation of expectation values and for further numerical analysis.

Chapter 5

Numerical Results and Discussions

5.1 $\mathbb{Z}_4$ Symmetries of Semionic RVB state Tensor Network

Symmetry properties of PEPS can be used to describe its topological order [14]. A PEPS can be defined as invariant under the action of the symmetry group G if for every $g \in G$, and for the local tensor S used to describe PEPS, S remains invariant under the action of g on all its virtual indices. G-invariance of S can be shown as:

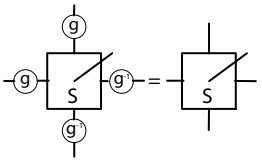

In case of RVB state topological order is accompanied by the invariance of tensor S under $\mathbb{Z}_2 = \{Z, I\}$ [4]. S also shows invariance in the case of Semionic RVB state but under the cyclic group $\mathbb{Z}_4 = \{\zeta, \zeta^2, \zeta^3, \zeta^4\} = \{\zeta, Z, \bar{\zeta}, I\}$. Generator ζ of $\mathbb{Z}_4$ is given by the following representation:

$$\zeta := \underbrace{\begin{pmatrix} 1 & 0 & 0 \\ 0 & 1 & 0 \\ 0 & 0 & i \end{pmatrix}}_{\eta} \otimes \underbrace{\begin{pmatrix} 0 & 1 \\ 1 & 0 \end{pmatrix}}_{flip} \tag{5.1}$$

where η acts on the legs of E tensor and $flip$ on δ tensor legs.

It can be shown analytically [15] that S remains invariant under the action of ζ on the outer legs of S which belong to the E and δ tensors.

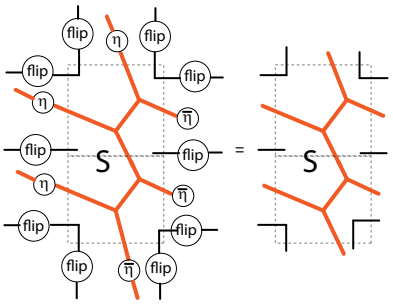

where black lines mark δ tensor legs and orange lines represent the legs of E.

In the following we give a sketch of the proof for $\mathbb{Z}_4$ invariance of the S tensors of Semionic RVB state.

Given the way we fix the boundary conditions (BC) called charges (as in the lattice gauge theory), we restrict possible lattice coverings or loop configurations between the two ends of the cylinder. All loop patterns with odd number of strings between the two ends of the cylinder and with color (δ) indices fixed by $|0\rangle \pm |1\rangle$ maps to $\pm i$ eigenspace of ζ. Similarly, all loop patterns with even strings and with color (δ) indices fixed by $|0\rangle \pm |1\rangle$ maps to ± 1 eigenspace of ζ. Action of ζ on these sub-spaces is shown below:

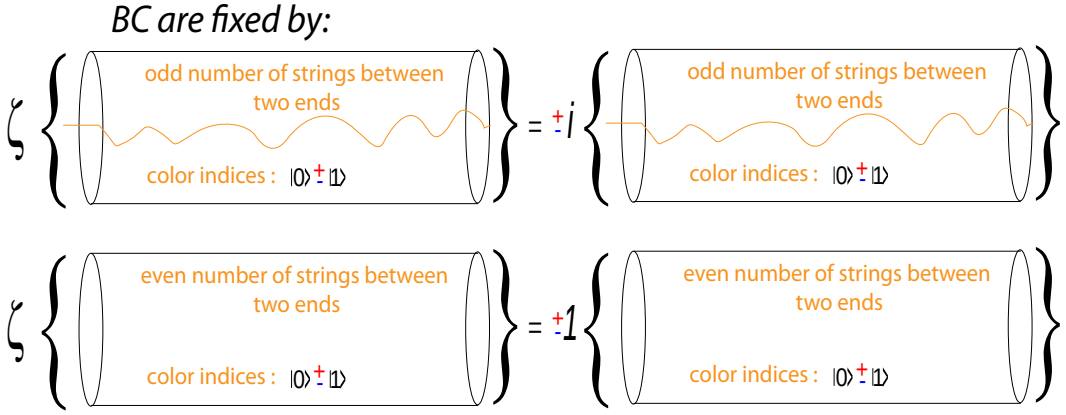

Each of the four sub-spaces are invariant the action of ζ and each one can be identified with one of the eigenvalues of ζ. Assuming these sub-spaces spans the space of all lattice coverings, it can be shown that ζ commutes with S. Using the same line of argument one can concludes that ζ commutes with S in the vertical direction. Thus, S is $\mathbb{Z}_4$ invariant.

Tensor $\mathbb{E}$ is also $\mathbb{Z}_4$ invariant since it is composed of $\mathbb{Z}_4$ invariant S tensors in the ket and bra layer. G-invariance property is stable under the concatenation of G-invariant tensors [14]. So, $\mathbb{T}$ is also $\mathbb{Z}_4$ invariant. $\mathbb{Z}_4$ symmetry of $\mathbb{T}$ translates into following

commutation relations.

$$[\mathbb{T}, 1 \otimes \zeta] = 0 \tag{5.2}$$

$$[\mathbb{T}, \zeta \otimes 1] = 0 \tag{5.3}$$

The commutation relations of $\mathbb{T}$ has also been varified numerically using following relation:

$$\left\| \left(\zeta^i\right)^{\otimes N_v} |v\rangle - \lambda |v\rangle \right\|_2 \longrightarrow 0 \tag{5.4}$$

where $|v\rangle$ are the eigenvectors of $\mathbb{T}$.

Given these commutation relations it can be inferred that $\mathbb{T}$ has a block diagonal form with 16 blocks. Each block of $\mathbb{T}$ corresponds to one of the irreducible representations of $\mathbb{Z}_4 \otimes \mathbb{Z}_4$ or to one of the eigenvalues of $\zeta^{\otimes N_v}$ for both the bra and ket layer of the transfer operator $\mathbb{T}$. If we include the flux lines (details given in the next section) then total transfer operator is made of 256 blocks in total.

$$\mathbb{T} = \bigoplus_{\phi,\phi'} \left\{ \bigoplus_{c,c'} \mathbb{T}_{\phi,c}^{\phi',c'} \right\} \tag{5.5}$$

where $c, c' \in \{1, -1, i, -i\}$ and $\phi, \phi' \in \{\zeta, Z, \overline{\zeta}, I\}$.

For a given PEPS one can define a parent Hamiltonian whose ground state subspace is spanned by the PEPS [14]. Given that the transfer operator $\mathbb{T}$ of PEPS has a block diagonal form, a lot of information about the parent Hamiltonian of the underlying PEPS can be read from the structure of these blocks. For instance, the number of blocks of $\mathbb{T}$ determines the degeneracy of the parent Hamiltonian [16].

5.2 Topological Sectors and Fixed Points of transfer operator $\mathbb{T}$

The manifold of Semionic RVB States contains all lattice coverings on the kagome lattice or loop patterns on its dual honeycomb. This space of possible configurations can be divided into different disconnected topological sectors. These sectors are topological since any local operator acting on a loop pattern preserves the sector and one can go from one sector to another only by nonlocal operations.

By fixing the charge $c \in \{1, -1, i, -i\}$ at the boundaries we choose one of the topological sectors $\mathcal{S}_c$. But $\mathcal{S}_c$ can be further divided into four sectors because ζ commutes with Semionic RVB state tensor S in the vertical direction also. For a given charge c, by inserting four different flux (as defined in lattice gauge theory) operators F_i, we can

create four different Semionic RVB states $\left|\chi_{(\zeta^i,c)}\right\rangle$ for charge c. Flux operators F_i are defined as:

$$F_i := \prod_{x \in C_x} \left(\zeta^i\right)_x \tag{5.6}$$

where $i \in \{1,2,3,4\}$ and $\zeta^2 = Z, \zeta^3 = \overline{\zeta}$ and $\zeta^4 = I$. C_x represents the sites where a string of ζ^i is inserted between the two ends of the cylinder as shown in *Fig. 5.1.*

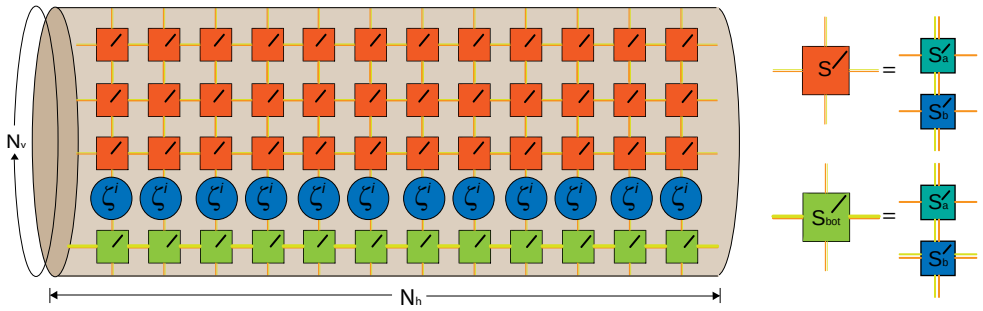

FIGURE 5.1: Tensor network of Semionic RVB state with flux ζ^i denoted by blue circles. N_v is equal to the number of $\mathbb{E}$ blocks along the circumference.

Depending on the value of i, flux operator F_i acts on each of the four sectors of $\mathcal{S}_c$ differently and generates corresponding phase factors. Phase factors generated by flux operators F_i for the four sectors of $\mathcal{S}_c$ is a topological property of the system since it is not effected by the location where the flux string is placed between the two ends of the cylinder.

We calculated largest eigenvalues $\gamma_{\phi,c}^{\phi',c'}$ of $\mathbb{T}$ for different flux lines ϕ, ϕ' and charges c, c' both in the ket and bra layer of $\mathbb{T}$ as shown in *Fig. 5.2.* Eigenvectors corresponding to the largest eigenvalues $\gamma_{\phi,c}^{\phi',c'}$ are the *fixed points of* $\mathbb{T}$ where topological sectors in the ket and bra layer are specified by the charges c and c' and superposition with in a topological sectors is given by fluxes ϕ and ϕ'.

On fixing the flux, $\mathbb{T}_{\phi}^{\phi'}$ has 16 blocks corresponding to different charges in ket and bra. Maximum eigenvalue $\gamma_{\phi,c}^{\phi',c'}$ for the block is evaluated by doing projection $P_c^{c'}$ after vector-$\mathbb{T}$ multiplication in each Lanczos iteration. $P_c^{c'}$ is a projector on the topological sectors c and c' in the ket and bra layer and is defined as:

$$P_c^{c'} := \sum_{i,j=1}^{4} \left(c \cdot \left(\zeta^{\otimes N_v}\right)\right)^i \otimes \left(c' \cdot \left(\zeta^{\otimes N_v}\right)\right)^j \tag{5.7}$$

There are 256 possible combinations of flux and charge. Due to reflection symmetry between ket and bra of $\mathbb{T}$, 136 combinations are sufficient to determine the eigenvalues for all possible combinations. Only certain combinations of (ϕ, ϕ', c, c') are compatible and the eigenvalues (fixed points) for the rest of the combinations are zero.

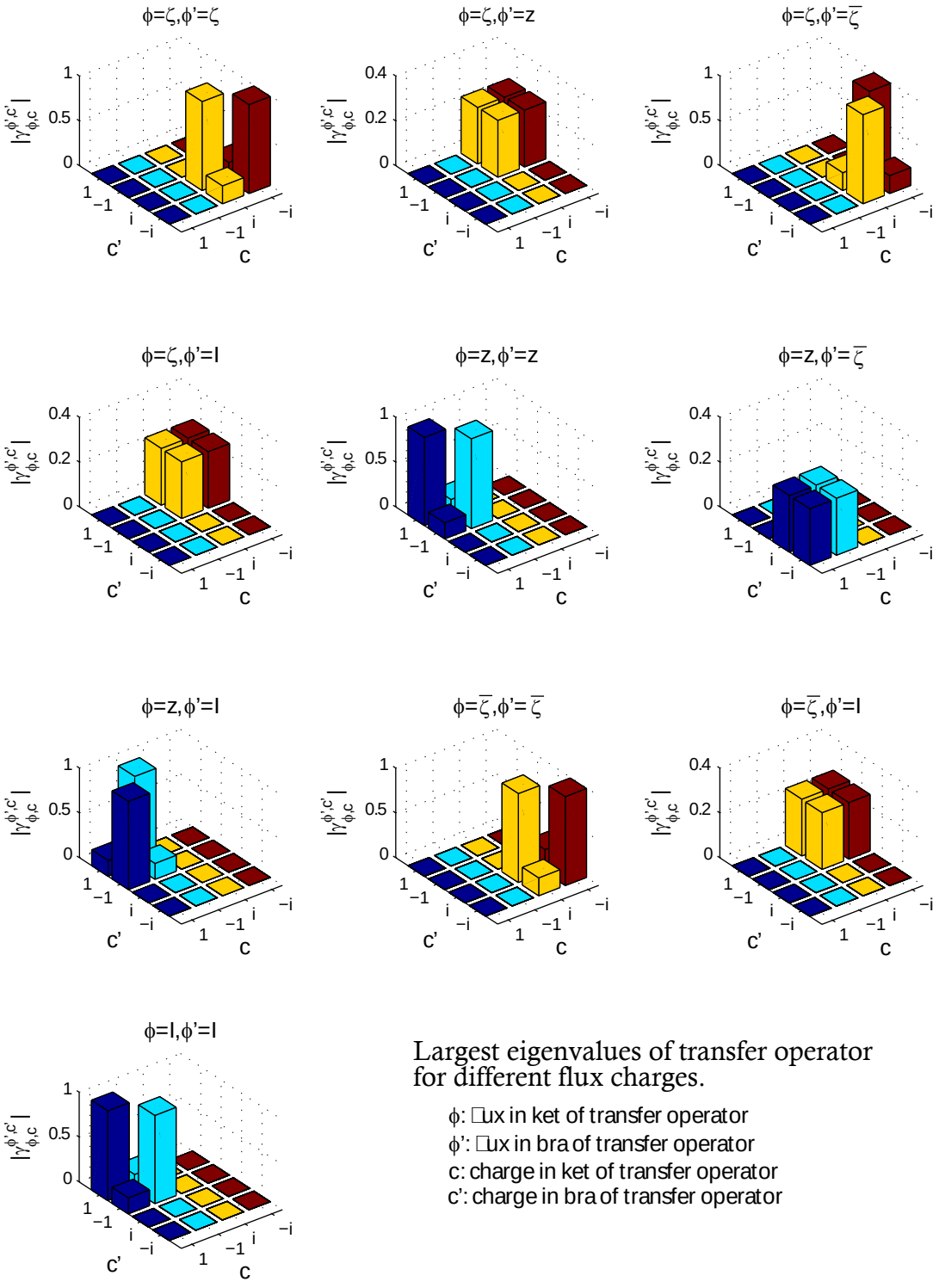

FIGURE 5.2: Largest eigenvalues (fixed points) of $\mathbb{T}$ for possible flux and charge combinations in the ket and bra layer, all values have been normalized by dividing by the largest eigenvalue.

5.3 Interpolation between Semionic RVB state and Double Semion model

Tensor network formalism allows us to do interpolation between two PEPS. One can determine whether the state these PEPS describe are in the same phase or not. The interpolation between two PEPS is in fact interpolation between linear maps $\mathcal{P}$, of respective PEPS by continuously deforming one map into another. We have studied the interpolation between Semionic RVB state and Semionic Dimer state (Double Semion model) by parametrizing $\mathcal{P}(\theta)$, such that

$$\mathcal{P}_\theta = \sum_{i=0}^{1} |i\rangle \left[\langle i2| \left(\langle \blacksquare\square| + \langle \square\blacksquare|\right) + \langle i2| \left(\langle \blacksquare\blacksquare| + \langle \square\square|\right)\right] + \theta \sum_{i=0}^{1} |i+2\rangle \left[\langle i2| \left(\langle \blacksquare\square| + \langle \square\blacksquare|\right) - \langle i2| \left(\langle \blacksquare\blacksquare| + \langle \square\square|\right)\right]. \tag{5.8}$$

It can be easily verified that,

$$\mathcal{P}_{srvb} \equiv \mathcal{P}_{\theta=0} = \sum_{i=0}^{1} |i\rangle \left[\langle i2| \left(\langle \blacksquare\square| + \langle \square\blacksquare|\right) + \langle i2| \left(\langle \blacksquare\blacksquare| + \langle \square\square|\right)\right] \tag{5.9}$$

and

$$\mathcal{P}_{dsem} \equiv \mathcal{P}_{\theta=1} = \sum_{i=0}^{1} \left(|i\rangle + |i+2\rangle\right) \left[\langle i2| \left(\langle \blacksquare\square| + \langle \square\blacksquare|\right)\right] + \left(|i\rangle - |i+2\rangle\right) \left[\langle 2i| \left(\langle \blacksquare\blacksquare| + \langle \square\square|\right)\right] \tag{5.10}$$

Varying θ between 0 to 1 is actually a way of making non-orthogonal dimer configurations in Semionic model to orthogonal configurations in the Double Semion model [4]. The results of interpolation for largest eigenvalues $\gamma_{\phi,c}^{\phi',c'}$ of $\mathbb{T}$ for different flux lines ϕ, ϕ' and charges c, c' both in the ket and bra layer of $\mathbb{T}$ are shown in *Fig. 5.3*.

Double semion model is equivalent to the Semionic Dimer state and it has four topological states as its ground state subspace. Only 12 distinct combinations of (ϕ, ϕ', c, c') remains non-zero at the Semionic Dimer state end of the interpolation and maps to its four topological states. All the remaining combinations decay to 0. These 12 distinct combinations is used in next section to construct Semionic RVB wavefunctions on the cylinder.

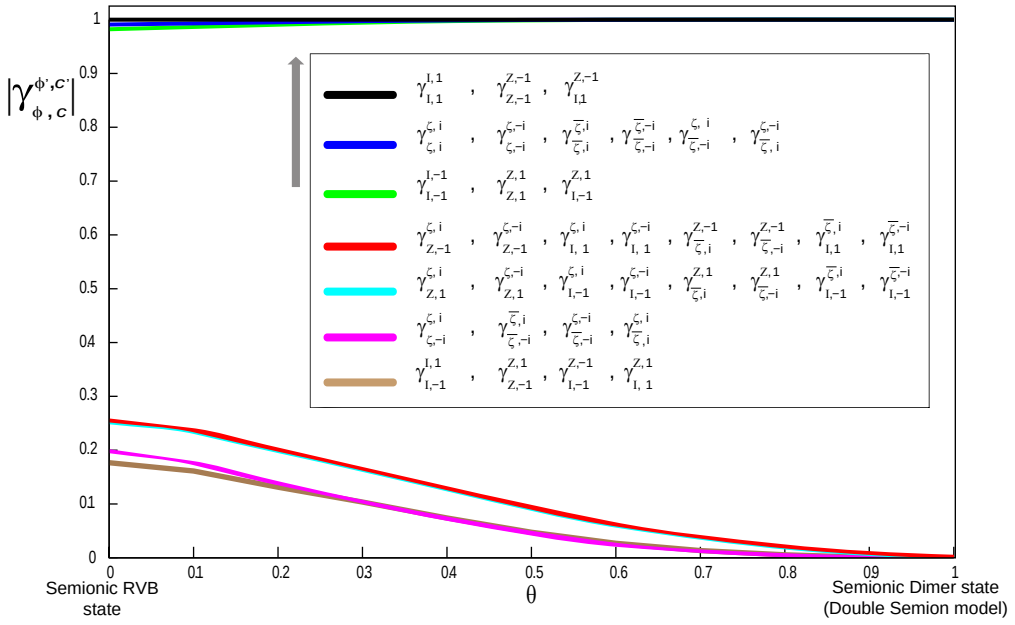

FIGURE 5.3: Interpolation between Semionic RVB state and Double Semion model for the largest eigenvalues of non-zero blocks of $\mathbb{T}$ corresponding to different flux-charge combinations in the ket and bra layer

5.4 Semionic RVB wavefunctions on the cylinder

From the numerical data of interpolation there are 12 distinct combinations for which the eigenvalues of $\mathbb{T}$ remains non-zero at Semionic Dimer state end of interpolation. These combinations are summarized below:

$$\gamma^{I,1}_{I,1} \quad \gamma^{Z,-1}_{Z,-1} \quad \gamma^{Z,-1}_{I,1}$$

$$\gamma^{\zeta,i}_{\zeta,i} \quad \gamma^{\bar{\zeta},-i}_{\bar{\zeta},-i} \quad \gamma^{\zeta,i}_{\bar{\zeta},-i} \quad \gamma^{\zeta,-i}_{\zeta,-i} \quad \gamma^{\bar{\zeta},i}_{\bar{\zeta},i} \quad \gamma^{\zeta,-i}_{\bar{\zeta},i}$$

$$\gamma^{I,-1}_{I,-1} \quad \gamma^{Z,1}_{Z,1} \quad \gamma^{Z,1}_{I,-1}$$

All combinations within one line generate same eigenvalue for the $\mathbb{T}$. State $|\chi_{(I,1)}\rangle$ in the bra layer when paired with itself or with the state $|\chi_{(Z,-1)}\rangle$ in the ket layer gives the same eigenvalue for $\mathbb{T}$. Largest eigenvalues $\gamma^{\phi',c'}_{\phi,c}$ of the transfer operator $\mathbb{T}$ for the combination (ϕ, ϕ', c, c') gives a measure of the overlap between the states $|\chi_{(\phi,c)}\rangle$ and $|\chi_{(\phi',c')}\rangle$. Since Cauchy–Schwarz inequality holds strictly equal for $\gamma^{Z,-1}_{I,1}$,$\gamma^{I,1}_{I,1}$, and $\gamma^{Z,-1}_{Z,-1}$, it suggests $|\chi_{(I,1)}\rangle$ and $|\chi_{(Z,-1)}\rangle$ are two equivalent ways for describing the same state. Following the same line of reasoning, one can identify four different states with alternate

representations.

$$\left.\begin{array}{l} \left|\chi_{(\zeta,i)}\right\rangle \leftrightarrow \left|\chi_{(\bar{\zeta},-i)}\right\rangle \\ \left|\chi_{(\bar{\zeta},i)}\right\rangle \leftrightarrow \left|\chi_{(\zeta,-i)}\right\rangle \\ \left|\chi_{(Z,1)}\right\rangle \leftrightarrow \left|\chi_{(I,-1)}\right\rangle \\ \left|\chi_{(I,1)}\right\rangle \leftrightarrow \left|\chi_{(Z,-1)}\right\rangle \end{array}\right\} \begin{array}{l} 4 \textit{ topologically} \\ \textit{degenerate states} \end{array} \tag{5.11}$$

These states corresponds to different charges (topological sectors) at the boundaries and type of flux strings between the two ends of cylinder.

5.5 Energy Density of Semionic RVB Wavefunctions and Topological order

Using fixed points corresponding to different topological sectors (charges) and fluxes, we computed energy density at the center of the cylinder in the limit $N_h \to \infty$. For a translationally invariant reference configuration R there are 12 distinct nearest neighbor interactions (couplings) between 6 sites in the tensor block S. Energy per site (density) is evaluated by doing the sum over all possible distinct couplings and dividing by number of sites. For different combinations of flux and charge in the ket and bra layer energy per site can be defined as:

$$E^{\phi',c'}_{\phi,c} = \frac{1}{6}\sum_{i=1}^{12} \frac{\left\langle \chi_{(\phi',c')} | h_{\infty,i} | \chi_{(\phi,c)} \right\rangle}{\left\langle \chi_{(\phi',c')} | \chi_{(\phi,c)} \right\rangle} \tag{5.12}$$

where $h_{\infty.i}$ is the local term of Heisenberg Hamiltonian at the center of infinite cylinder.

Energy per site for different combinations are shown in *Fig. 5.4*. From the analysis of data in *Fig. 5.4* different blocks of $\mathbb{T}$ corresponding to the states in [Eq. 5.11] can be ordered in the following way:

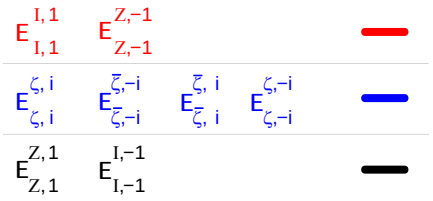

$E^{I,1}_{I,1}$ and $E^{Z,-1}_{Z,-1}$ denotes energy per site for the states $\left|\chi_{(I,1)}\right\rangle$ and $\left|\chi_{(Z,-1)}\right\rangle$ respectively. The results for energy density in case of RVB state and Semionic RVB state shows that RVB states gives lower energy density and makes a better ansatz for the ground state of anti-ferromagnetic Heisenberg Hamiltonian on kagome lattice as compared to the Semionic RVB states.

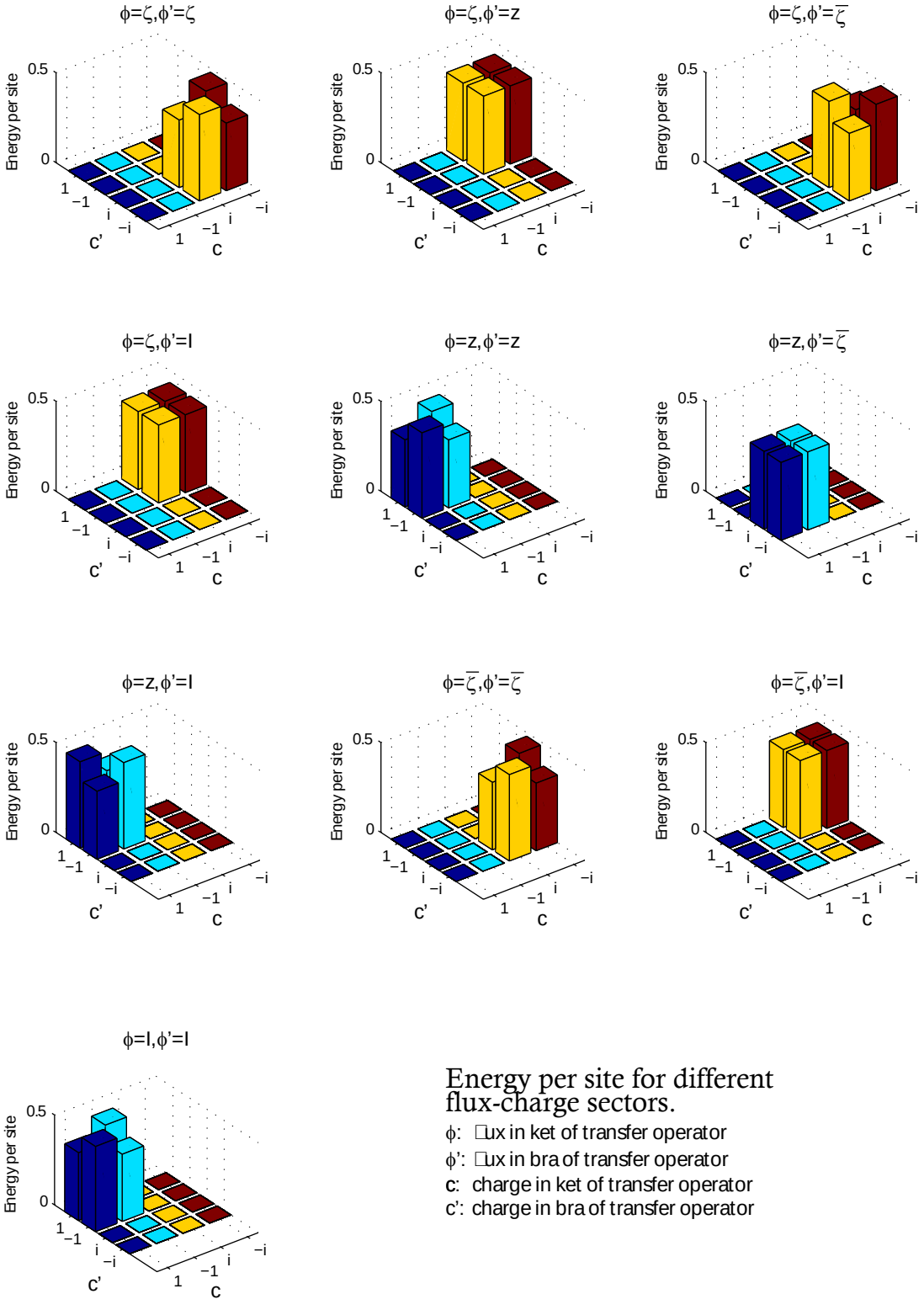

FIGURE 5.4: Energy per site calculated at the center of cylinder in the limit $N_h \to \infty$ for different fixed points determined by flux and charge combinations in the ket and bra layer $\mathbb{T}$.

Eigenvalues of transfer operator $\mathbb{T}$ for the four state in [Eq. 5.9] converge exponentially to the same value in the thermodynamic limit as $N_h, N_v \to \infty$ and this is shown in *Fig.5-5(a)*. Splitting between the maximum and minimum eigenvalue exponentially decay to zero *Fig.5-5(b)*.

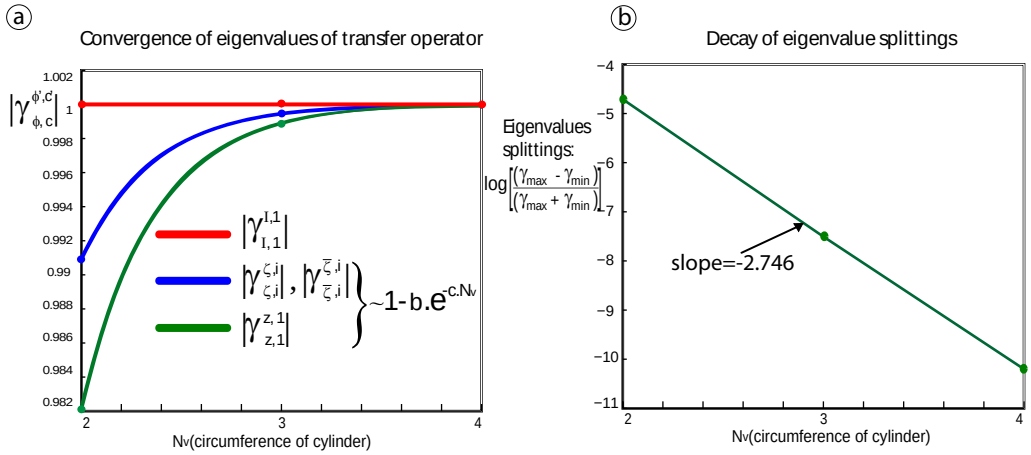

FIGURE 5.5: (a)Convergence of eigenvalues of $\mathbb{T}$ for the four states in [Eq. 5.9] in limit $N_h, N_v \to \infty$. Data points have been fitted with $1 - be^{-cN_v}$. For blue line b=2.404 and c=2.79, for green line b=4.683 and c=2.785, for green line b=0. and c=0.(b) Decay of eigenvalue splittings: $\log\left(\frac{(\gamma_{max}-\gamma_{min})}{(\gamma_{max}+\gamma_{min})}\right)$.

Calculations of energy per site for the four states at the center of infinite cylinder as $N_v \to \infty$ also shows a similar behavior. Energies of the four states exponentially converge *Fig.5-6(a)* and the splittings between the energies exponentially decays to zero *Fig.5-6(b)*.

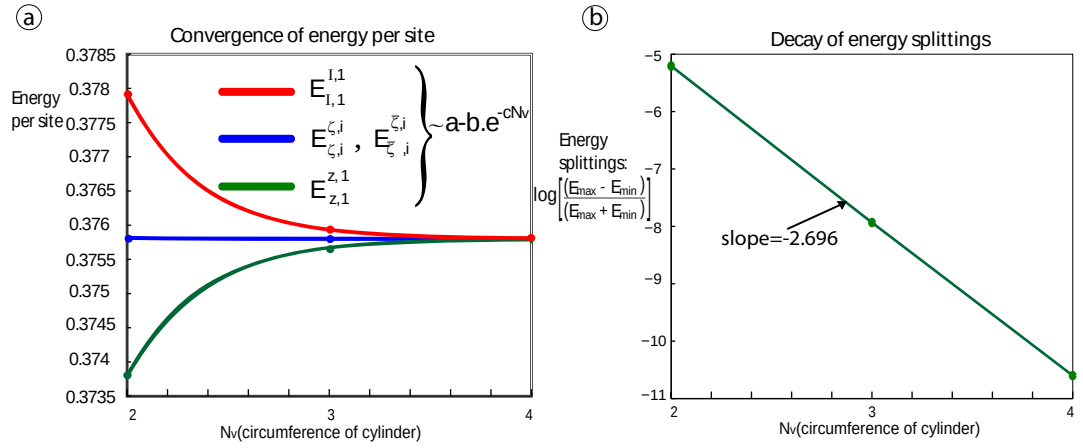

FIGURE 5.6: (a)Convergence of energy density for the Semionic RVB states[Eq. 5.9] in limit $N_h, N_v \to \infty$. Data points have been fitted with $a - be^{-cN_v}$. For blue line a=0.3758, b=-0.0116, c=3.365, for green line a=0.3758, b=0.4527, c=2.71, and for red a=0.3758, b=-0.5204, c=2.753. (b)Decay of energy splittings: $\log\left(\frac{(E_{max}-E_{min})}{(E_{max}+E_{min})}\right)$.

Convergence of the eigenvalues and energies gives a strong evidence that the four Semionic RVb states [Eq. 5.9] are topologically degenerate since each state looks locally the same.

Measurement of any local order parameter cannot distinguish between any of the four degenerate states.

5.6 Reference Configurations

Each block S in the tensor network of Semionic RVB state contains 6 physical sites. For each physical site their are two possibilities, depending on whether or not it is a dimer site. So, there are $2^6 = 64$ possibilities. Out of 64 only 8 can be valid reference configurations, the rest of them violates the parity constraints enforce by the Arrow rule. 8 possible reference configurations are shown in the *Fig. 5-7.* The two reference configurations in each column are related to each other by translation.

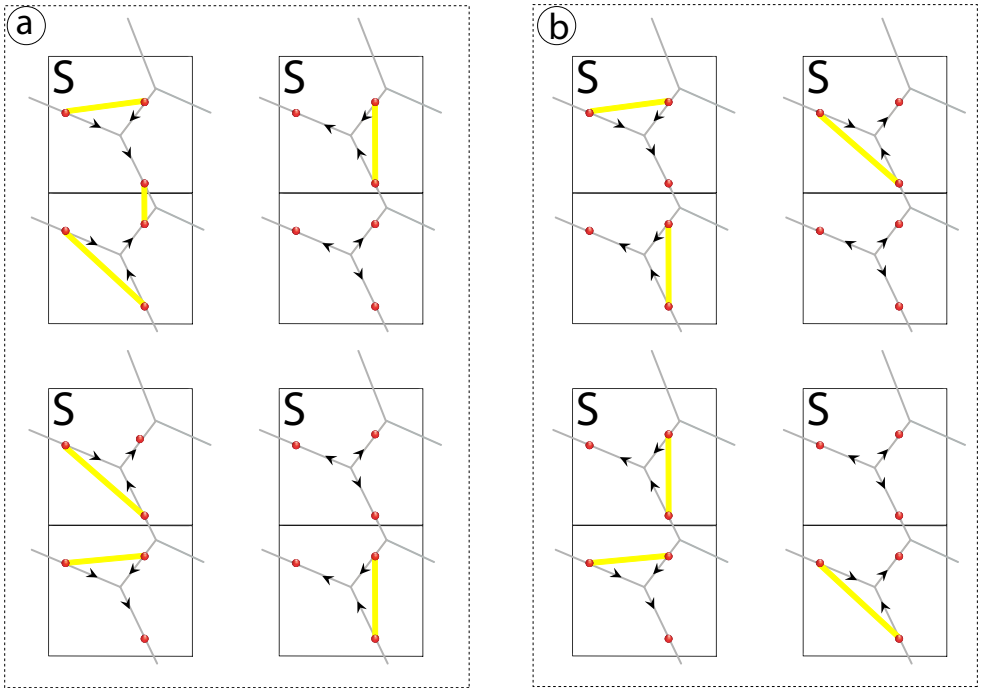

FIGURE 5.7: All possible reference configurations. Red dots represent the physical site and yellow lines mark dimers. All dimers that extend to the outside of the box are not shown.

All the calculations for the fixed points of transfer operator, interpolation between Semionic RVB state and Semionic Dimer state, and energy per site as shown on the previous pages has been done for top left reference configuration in box.a of *Fig. 5-7.*

Given a flux-charge combination in the ket and bra layer of $\mathbb{T}$, for all reference configurations within box a. of *Fig. 5-7.* the calculations of fixed points (eigenvalues) of $\mathbb{T}$ give same results. The aforementioned statement also holds true for reference configurations within box b. of *Fig. 5-7.* But the results for reference configuration within box a.

and box b. differ from each other. The reason for this discrepancy is still not clearly understood.

Chapter 6

Summary

In this thesis we presented a PEPS and Tensor Network formalism of Semionic RVB state by extending on the arrow interpretation of Normal RVB states. Given the time and space complexity of the tensor network for Semionic RVB state we introduced two optimizations in [sec. 4.3] these optimizations allowed us to do numerics for these states with upto four blocks along the circumference of the cylinder.

We tried to asses whether Semionic RVB states can appear ground states of Heisenberg Hamiltonian on kagome lattice. In [sec. 5.1] we analyzed symmetries in tensor network of Semionic RVB state and showed that it is $\mathbb{Z}_4$ invariant. In [sec. 5.2] we parametrized four topologically degenerate Semionic RVB states and study their topological order. The comparisons of results for energy density in case of RVB state and Semionic RVB state shows that RVB states makes a better ansatz for the ground state of anti ferromagnetic Heisenberg Hamiltonian on kagome lattice. The results of interpolation in [sec. 5.3] between Semionic RVB state and Semionic Dimer state show that Semionic RVB state is in the same phase as Double Semion Model and realizes a $\mathbb{Z}_2$ spin liquid state. The question of dependency of results on different reference configuration still remained to be answered.

Appendix A

Toric Code state and Double Semion Model

This appendix gives a brief overview of Toric code state and Double Semion Model. It does not attempt to prove any new result and mostly based on the work of Levin and Wen in [13, 17]. Toric code model and Double Semion model are simplest examples of string-net condensed state. They are the ground states of exactly soluble Hamiltonains of the form [17]:

$$H = -\sum_{\mathbf{v}} Q_{\mathbf{v}} - \sum_{\mathbf{p}} B_{\mathbf{p}} \tag{A.1}$$

where $\mathbf{v}$ runs over all the vertices and $\mathbf{p}$ runs over all the plaquettes (hexagons) of the honeycomb lattice. Local terms $Q_{\mathbf{v}}$ and $B_{\mathbf{p}}$ are called the electric charge and magnetic flux operators.

These Hamiltonians provide an explicit realization of topological phases.

A.1 Toric code Model

Given a system of spin-1/2 at the links of honeycomb lattice, acts the Hamiltonian:

$$\mathcal{H}_{tc} = -\sum_{\mathbf{v}} \left(\prod_{i \,\in\, vertex(\mathbf{v})} \sigma_i^z \right) - \sum_{\mathbf{p}} \left(\prod_{j \,\in\, plaquette(\mathbf{p})} \sigma_j^x \right) \tag{A.2}$$

where $\sigma^{x,z}$ are Pauli matrices. The first term (electric charge) acts on three legs of vertex $\mathbf{v}$, the second term magnetic energy acts on the six edges of $\mathbf{p}$ with an operator σ^x.

The ground state of this model is exactly known. The ground state of $\mathcal{H}_{tc}$ can be understood in the language of string nets. We define *strings* as the links of the honeycomb

lattice where physical sites has $\sigma^z = -1$, sites with $\sigma^z = 1$ are treated as empty. The first term in the $\mathcal{H}_{tc}$ is minimized by an even number of down spins around a vertex. The second terms flip all the spins in the plaquette. So, ground state $|\psi_{tc}\rangle$ of $\mathcal{H}_{tc}$ can be interpreted as an equal weight superposition of all possible closed string loop configurations [13].

$$|\psi_{tc}\rangle = \sum_{L \in \text{closed}} |L\rangle \tag{A.3}$$

Manifold of all possible closed string configurations can be divided into four disconnected topological sectors. Each sector is characterized by winding number parity P_x and P_y:

$$P_{x/y} = \prod_{i \in C_{x/y}} \sigma_i^z \tag{A.4}$$

where $C_{x/y}$ represents links along the blue line as shown in *Fig. A.1.*

Toric code is a simplest model of $\mathbb{Z}_2$ lattice gauge theory. $|\psi_{tc}\rangle$ contains topological order which breaks no symmetry. It has quasi-particle excitations with non-trivial statistics, and non-zero entanglement entropy.

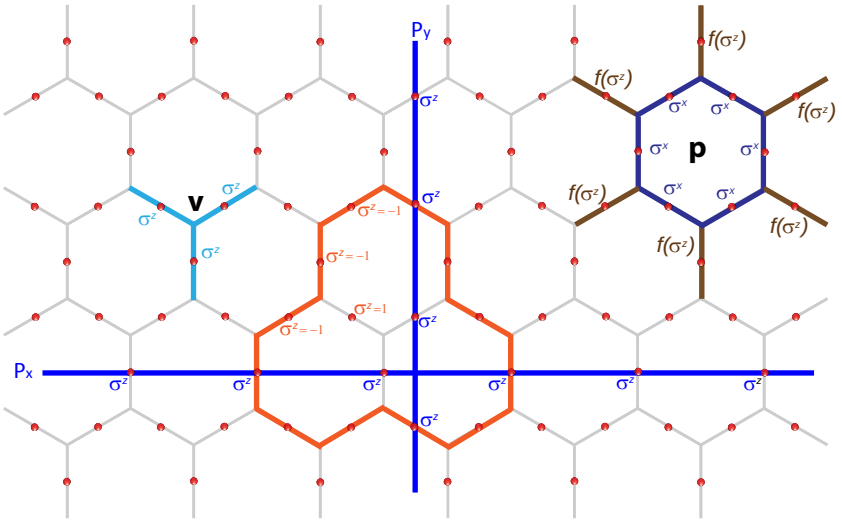

FIGURE A.1: Honeycomb lattice with physical sites marked by red dots. Legs of vertex **v** are denoted by light blue lines that are acted on by σ_z. Plaquette **p** is acted at the edges with σ_x. Legs of **p** are operated on by $f(\sigma^z)$ which is I in case of Toric code model and $i^{(1-\sigma^z)/2}$ in the case of Double Semion model. Dark blue lines with string of σ_z's represent winding number parity operators P_x/y. Loop marked by orange lines represent strings on physical sites with $\sigma_z = -1$ [22].

A.2 Double Semion Model

Double Semion Model was introduced by Levin and Wen in [17]. It is the ground state of the Hamiltonian:

$$\mathcal{H}_{dsem} = -\sum_{\mathbf{v}} \left(\prod_{i \,\in\, vertex(\mathbf{v})} \sigma_i^z \right) + \sum_{\mathbf{p}} \left(\prod_{j \,\in\, plaquette(\mathbf{p})} \sigma_j^x \right) \left(\prod_{j \,\in\, legs(\mathbf{p})} i^{\left(1-\sigma_j^z\right)/2} \right) \tag{A.5}$$

Similar to the Toric code, first term (electric charge) acts on three legs of vertex $\mathbf{v}$, the second term magnetic energy acts on the six edges of $\mathbf{p}$ with an operator σ^x and on six legs of $\mathbf{p}$ with an operator $i^{\left(1-\sigma_j^z\right)/2}$ (see *Fig. A-1*). The ground state of Double semion model also know exactly and can be interpreted in the string language. Ground state of $\mathcal{H}_{dsem}$ is a superposition of all possible string configurations with different phase factors that are determined by the parity of the number of closed strings in the loop configurations configurations [13].

$$|\psi_{dsem}\rangle = \sum_{L \,\in\, closed} (-1)^{n(L)} |L\rangle \tag{A.6}$$

where $n\,(L)$ is the number of closed strings in the loop configuration.

Double semion state contains topological order that is characterized by quasi-particle excitations with semionic statistics and long range entanglements.

Although, Toric code state and Double Semion state are made of long range objects (string configurations) that extend up to the size of the system, and $n\,(L)$ is a global property which cannot by determined locally, both of them have efficient Tensor Network description in terms of local tensors [13]. Hidden within these states are Quantum Dimer models which are defined by loop patterns made by the overlap of dimer coverings with any arbitrary dimer configuration. Toric code and Double Semion model present a dual picture of Dimer state and Semionic dimer state respectively.

Bibliography

[1] Claudine Lacroix, Philippe Mendels, Frederic Mila, Introduction to Frustrated Magnetism Materials, Experiments, Theory, Springer Heidelberg (2010)

[2] A. Yu. Kitaev, Fault-tolerant quantum computation by anyons, arXiv:quant-ph/9707021 (1997)

[3] Topological and entanglement properties of resonating valence bond wave functions, D Poilblanc, N Schuch, D Pérez-García, JI Cirac, Physical Review B 86, 014404 (2012)

[4] N Schuch, D Poilblanc, JI Cirac, D Perez-Garcia, Resonating valence bond states in the PEPS formalism, Phys. Rev. B 86, 115108 (2012)

[5] D Poilblanc, N Schuch, Simplex $\mathbb{Z}_2$ spin liquids on the kagome lattice with projected entangled pair states: Spinon and vison coherence lengths, topological entropy, and gapless edge modes, Phys. Rev. B 87, 140407(R) (2013)

[6] N Schuch, Condensed Matter Applications of Entanglement Theory, Quantum Information Processing. Lecture Notes of the 44th IFF Spring School (2013)

[7] Roman Orus,A Practical Introduction to Tensor Networks:Matrix Product States and Projected Entangled Pair States, arXiv:1306.2164 (2013)

[8] M. B. Hastings, Solving Gapped Hamiltonians Locally, arXiv:cond-mat/0508554 (2005)

[9] F. Verstraete, M. M. Wolf, D. Perez-Garcia, and J. I. Cirac, Criticality, the Area Law, and the Computational Power of Projected Entangled Pair States, Phys. Rev. Lett. 96, 220601 (2006)

[10] Yuan Wan and Oleg Tchernyshyov, Phenomenological $\mathbb{Z}_2$ lattice gauge theory of the spin-liquid state of the kagome Heisenberg antiferromagnet, arXiv:1301.5008 (2013)

[11] G. Misguich,D. Serban, and V. Pasquier, Quantum Dimer Model on the Kagome Lattice: Solvable Dimer Liquid and Ising Gauge Theory, arXiv:cond-mat/0204428 (2002)

[12] Veit Elser and Chen Zeng, Kagome spin- 1/2 antiferromagnets in the hyperbolic plane, Phys. Rev. B 48, 13647–13653 (1993)

[13] Zheng-Cheng Gu, Michael Levin, Brian Swingle, and Xiao-Gang Wen, Tensor-product representations for string-net condensed states, Phys. Rev. B 79, 085118 (2009)

[14] PEPS as ground states: degeneracy and topology, N Schuch, I Cirac, D Perez-Garcia, arXiv:1001.3807 (2010)

[15] Norbert Schuch showed the proof steps in a private conversation.

[16] Norbert Schuch, Didier Poilblanc, J. Ignacio Cirac, David Perez-Garcia, Topological order in PEPS: Transfer operator and boundary Hamiltonians, Phys. Rev. Lett. 111, 090501 (2013)

[17] Michael A. Levin and Xiao-Gang Wen, String-net condensation: A physical mechanism for topological phases, arXiv:cond-mat/0404617 (2004)

[18] Xiao-Gang Wen, An Introduction of Topological Orders, *http* : *//dao.mit.edu/ wen/topartS*3*.pdf*

[19] John B. Parkinson and Damian J.J. Farnell, An Introduction to Quantum Spin Systems, Springer Heidelberg (2010)

[20] F. Verstraete, J.I. Cirac, and V. Murg, Matrix Product States, Projected Entangled Pair States, and variational renormalization group methods for quantum spin systems, arXiv:0907.2796 (2009) http://arxiv.org/abs/1008.3477

[21] D. Perez-Garcia, F. Verstraete, M.M. Wolf, and J.I. Cirac, Matrix Product State Representations, arXiv:quant-ph/0608197 (2006)

[22] *Fig. 3.2* and *Fig. A.1* have been drawn with an idea from *Fig. 31* in [5] and from *Fig. 12* in [15] respectively.

[23] D.S. Rokhsar and S.A. Kivelson, Superconductivity and the Quantum Hard-Core Dimer Gas, Phys. Rev. Lett. 61, 2376 (1988)

[24] Norbert Schuch, Michael M. Wolf, Frank Verstraete, J. Ignacio Cirac, The computational complexity of PEPS, arXiv:quant-ph/0611050 (2006)

Acknowledgements

I am deeply grateful to my advisor, Norbert Schuch for mentoring me during the whole period of thesis. Thank you for your patience to answer all my questions and for making sense of things I find incomprehensible, you are truly an inspiration to me and I feel lucky that I had an advisor like you.

I owe a debt of gratitude to Gregor Bransky for helping me in reviewing the thesis text and for being such a wonderful office mate. I would to thanks all the students, postdocs, faculty members, and specially secretary Helene Barton at the Institute for Quantum Information for creating such a healthy work environment.

Thanks to my friend Jamshaid Ali for keeping me occasionally distracted to his problems, and for wonderful conversations. And special thanks to my parents and to my sisters for everything they have done for me.